JOURNAL OF PETROLOGY | VOLUME 52 | NUMBERS 7 & 8 | PAGES 1281–1305 | 2011 | doi:10.1093/petrology/egq081

Silicate–Carbonate Liquid Immiscibility and Phase Relations in the System SiO_2–Na_2O–Al_2O_3–CaO–CO_2 at 0·1–2·5 GPa with Applications to Carbonatite Genesis

R. A. BROOKER[1]* AND B. A. KJARSGAARD[2]

[1]SCHOOL OF EARTH SCIENCES, UNIVERSITY OF BRISTOL, WILLS MEMORIAL BUILDING, QUEENS ROAD, BRISTOL BS8 1RJ, UK

[2]GEOLOGICAL SURVEY OF CANADA, 601 BOOTH STREET, OTTAWA, ON, CANADA K1A 0E8

RECEIVED MARCH 1, 2010; ACCEPTED NOVEMBER 9, 2010
ADVANCE ACCESS PUBLICATION DECEMBER 24, 2010

We present new experiments, combined with a re-evaluation of published data, to characterize the topology of the silicate–carbonate two-liquid solvus in the five-component system SiO_2–Na_2O–Al_2O_3–CaO–CO_2 ($SNAC + CO_2$). Conjugate liquid compositions have been determined for a wide range of pressures (0·1–2·5 GPa) and temperatures (1225–1700°C) as well as variable degrees of CO_2 saturation. The expansion of the two-liquid field with increasing pressure and/or decreasing temperature, and the contraction of the two-liquid field for conditions where $P_{CO2} < P_{total}$ is accurately presented for the first time. The shape of the two-liquid solvus suggests that alkali-rich carbonatites can have a range of $SiO_2 + Al_2O_3$ contents down to very low values (<1 wt %), but that low-alkali or alkali-free immiscible carbonatites will always have $SiO_2 + Al_2O_3$ contents greater than 10–15 wt %. The most commonly observed carbonatite rock compositions observed at the Earth's surface all tend towards low contents of alkalis SiO_2 and Al_2O_3 and would have fractionated silicate phases from the carbonatite parental melts, possibly associated with alkali loss to coexisting fluids. Our results also show that carbonate liquid exsolution can occur from a CO_2-undersaturated ($P_{CO2} < P_{tot}$) silicate melt. Although the expanded high-pressure miscibility gap appears favourable for producing natural silicate melt compositions, a low-pressure (<1·0 GPa) magma chamber in the crust or perhaps in the shallow mantle below a rift provides the most likely environment for immiscibility to arise owing to the lower CO_2 demand of the silicate magma. Unusual textures in some experiments, suggestive of a deformable liquid state for the $CaCO_3$ phase, are conclusively shown to be characteristic of a non-quenchable, high-temperature polymorph of solid calcite. Similar calcite globules with this rounded appearance, which are also observed in some nephelinite lavas and mantle xenoliths, must be solid calcite and not immiscible liquids. This is consistent with the high $SiO_2 + Al_2O_3$ requirement of low-alkali or alkali-free immiscible carbonate liquids.

KEY WORDS: *carbonatite; experimental petrology; immiscibility*

INTRODUCTION

Numerous experimental studies on silicate–carbonate liquid immiscibility have been undertaken during the past four decades, and the results have been used to speculate on the origin of carbonatite magmas. Liquid immiscibility is a particularly attractive petrogenetic model, given the apparent bimodal distribution of rock types at numerous alkaline silicate–carbonatite complexes (e.g. Le Bas, 1987), and is currently the favoured mechanism for a number of localities including Oldoinyo Lengai (Freestone & Hamilton, 1980; Kjarsgaard *et al.*, 1995; Veksler *et al.*, 1998; Mitchell, 2009), Shombole (Kjarsgaard & Peterson, 1991; Kjarsgaard, 1998), Kerimasi (Guzmics *et al.*, 2010), the Gardiner complex (Nielsen, 1980) and Gronnedal–Ika (Halama *et al.*, 2005). However, ~25% of all carbonatites worldwide have no associated silicate rocks (Woolley &

*Corresponding author. Telephone: (44) 117 954 5377. Fax: (44) 117 925 3385. E-mail: richard.brooker@bristol.ac.uk

Kjarsgaard, 2008), and it is difficult to invoke exsolution from a silicate magma as a viable process for these occurrences. The two other main petrogenetic hypotheses for the generation of carbonatite magmas involve partial melting of a carbonated mantle peridotite (e.g. Wallace & Green, 1988; Gittins, 1989; Dalton & Wood, 1993; Moore & Wood, 1998; Brey *et al.*, 2009) or extensive fractionation of a silicate magma to produce a late-stage, carbonate-rich liquid (e.g. Watkinson & Wyllie, 1971; Lee & Wyllie, 1994, 1998). There are a number of pitfalls associated with all three of these models (e.g. Bell *et al.*, 1998). For example, the most common alkali-free carbonatite compositions have not been reproduced by immiscibility in experiments, the low-degree direct mantle melts may have problems being extracted from the mantle source and passing a thermal barrier ('ledge'), and extensive fractionation to produce carbonate precipitating melts results in high crystal fractions that make the magmas difficult to intrude. It is also possible that carbonatites exposed at the Earth's surface are generated in a range of environments from the mantle to the shallow crust, via a variety of processes rather than just one. Hence it is important to fully investigate each of these three postulated petrogenetic processes over an extensive range of pressure–temperature conditions using laboratory experiments. In this study we investigate the two-liquid miscibility gap (solvus) and phase relations in the simple system SiO_2–Na_2O–Al_2O_3–CaO (SNAC) + CO_2 at crustal to upper mantle conditions (0·1–2·5 GPa; *c.* 3–80 km depth). We report the results of over 80 experiments, providing analyses of silicate and carbonate liquids, as well as 29 bulk CO_2 determinations on silicate glasses.

We note that the geological literature on liquid immiscibility has been guilty of using the incorrect term 'two-liquid solvus' when in fact a solvus can only technically apply to a solid solution. Binodal, binodal curve and binodal surface are the correct terms for coexisting liquids or fluids. However, as most researchers in this field are familiar with the term solvus we continue to use this here. Also, to make descriptions clearer we refer to several 'solvi', which may be incorrect as they are often different traces of a single solvus (or binodal) surface. We have used the term 'quasi-ternary' as opposed to 'pseudo-ternary' as this avoids the mixing of Greek and Latin origins in the latter and the meaning is clear.

PREVIOUS EXPERIMENTAL STUDIES ON SILICATE–CARBONATE LIQUID IMMISCIBILITY

Simple analogue systems

Numerous experimental studies have used the SNAC + CO_2 system as an analogue to model the conditions required for silicate–carbonate liquid immiscibility (e.g. Koster van Groos & Wyllie, 1966, 1968, 1973; Kjarsgaard & Hamilton, 1988, 1989*a*; Brooker & Hamilton, 1990; Lee & Wyllie, 1994, 1996, 1997*a*). The SNAC system has a number of experimental advantages over natural compositions. In particular, the absence of Fe reduces the need to control fO_2 and eliminates problems of iron loss to capsule materials; the exclusion of MgO minimizes the precipitation of solid phases, which can complicate textural interpretations. Another advantage is the limited number of components, allowing for more accurate graphical representation of the experimental data on phase diagrams. The disadvantages include unrealistically high liquidus temperatures and precipitation of minerals that are not observed in natural carbonatite complexes (e.g. scapolite, plagioclase). These factors, combined with the difficulty in graphically comparing simple and complex natural compositions, can lead to problems in relating the experimental results to whole-rock geochemical and mineral chemistry data from natural rocks.

Studies in the 1960s and 1970s by Wyllie and co-workers at moderate to high alkali contents established the silicate–carbonate two-liquid field in the SNAC + CO_2 ($\pm H_2O$) system, but suggested that immiscibility was confined to very high-alkali compositions, that are not representative of natural Ca-rich carbonatites. However, subsequent experimental studies in more complex multicomponent systems (Koster van Groos, 1975; Verwoerd, 1978; Freestone & Hamilton, 1980) indicated that a two-liquid field exists to much lower alkali compositions.

Kjarsgaard & Hamilton (1988, 1989*a*) were the first to suggest an even larger two-liquid field in the SNAC + CO_2 system, extending to alkali-free compositions at 0·2 and 0·5 GPa. In the experiments of Kjarsgaard & Hamilton (1988, 1989*a*) an almost pure $CaCO_3$ phase was interpreted as a liquid, thus giving an analogue composition comparable with many natural low-alkali, silica-free calciocarbonatites. Subsequent experiments in the SNAC + CO_2 system at 1·5 GPa by Brooker & Hamilton (1990) were interpreted as containing three immiscible liquids: silicate liquid, Ca–Na carbonate liquid and an almost pure $CaCO_3$ liquid. Because all previous studies illustrated the expansion of the two-liquid solvus with increasing pressure, the extension of the two-liquid field to alkali-free compositions in the SNAC + CO_2 system was, in part, reconcilable with the smaller two-liquid fields observed in the earlier, low-pressure (0·1 GPa) studies. In a study of CO_2-saturated SNAC melts of sodamelilite composition ($NaCaAlSi_2O_7$), Mattey *et al.* (1990) showed the expansion of the two-liquid solvus with increasing pressure for this relatively low alkali bulk composition, with one liquid at 0·5–1·0 GPa, but two liquids at 2·0 and 3·0 GPa. Lee & Wyllie (1996) studied nine bulk composition along the albite (Ab)–calcite (Cc) join at 1·0, 1·5 and 2·5 GPa, and provided analyses

of quenched conjugate liquids from seven experiments at 2·5 GPa. Silicate (3·7–7·8 wt % Na_2O) and carbonate (5·3–11·8 wt % Na_2O) liquids all have low alkali contents. Based on these experiments, Lee & Wyllie (1996) suggested a significant expansion of the two-liquid field from 1·0 to 2·5 GPa, and provided a schematic interpretation of the two-liquid field in $SiO_2 + Al_2O_3 - Na_2O - CaO$ space at 1·0 and 2·5 GPa, utilizing conjugate liquid pair compositions from previous studies undertaken with moderate- to high-alkali bulk compositions.

Preliminary reports for experiments in the alkali-free system SiO_2–Al_2O_3–MgO–$CaO + CO_2$ by Novella & Kershav (2010) have identified two liquids at 2·0–2·6 GPa, suggesting that the two-liquid field expands all the way to alkali-free compositions.

Natural compositions

Experiments utilizing natural rock powders from Oldoinyo Lengai (Freestone & Hamilton, 1980; Kjarsgaard *et al.*, 1995) and Shombole (Kjarsgaard & Peterson, 1991; Hamilton & Kjarsgaard, 1993; Kjarsgaard, 1998), at pressures from 0·07 to 0·76 GPa, observed that the miscibility gap closed off at low alkali contents, before reaching alkali-free compositions. Experiments at 0·2 GPa utilizing eight- to ten-component synthetic systems also observed solvus closure at low alkali concentrations (Suk, 2001, 2003). These experimental studies all confirmed an increase in the size of the two-liquid field with increasing pressure or deceasing temperature. In contrast to results that show an expansion of the two-liquid solvus, Baker & Wyllie (1990) observed a very small two-liquid field at 2·5 GPa, and based on this and further results in a synthetic nephelinite–carbonate system, Lee & Wyllie (1997*b*) suggested a decrease in the two-liquid field in higher pressure experiments and attributed this to an increased MgO content. A re-examination of the Baker & Wyllie experiments by Brooker (1998) concluded that the decreased size of their two-liquid field resulted from a low bulk CO_2 content in the starting composition leading to CO_2 undersaturation in these experiments (i.e. $P_{CO2} < P_{total}$). The use of graphite liners in experiments with natural (Fe-bearing) compositions (e.g. Baker & Wyllie, 1990; Lee & Wyllie, 1997*b*) may also have led to further CO_2 undersaturation, as CO can be produced to dilute any excess fluid. Experiments by Dasgupta *et al.* (2006) examined melts formed in equilibrium with a simulated mantle assemblage at 3·0 GPa and found a wide two-liquid field at very low (<2 wt %) alkali contents. These 3·0 GPa results are consistent with the expanding high-pressure field shown by the SNAC + CO_2 data and the alkali-free results of Novella & Kershav (2010). Wallace & Green (1988) also noted apparent immiscible textures in their study of carbonated peridotite melting at 3·1 GPa, although no compositions were reported.

Solid calcite and carbonate liquids

Historically, the determination of the true extent of the two-liquid field has been complicated by the interpretation of 'pure $CaCO_3$ globules', which appear to have liquid-like textures. In particular, for low-alkali and alkali-free SNAC + CO_2 experiments, the suggestion has been made that that two-liquid pairs with conjugate $CaCO_3$ liquid 'globules' indicate that the solvus does not close off at low alkali contents in experiments at low pressures (0·2 and 0·5 GPa). This textural interpretation, originally made by Kjarsgaard & Hamilton (1988, 1989*a*), was subsequently reinterpreted by Kjarsgaard, and a revised phase diagram was presented in fig. 5b of Macdonald *et al.* (1993) with the $CaCO_3$ 'globules' being reinterpreted as a solid phase and the two-liquid field being closed off at low alkali compositions. Lee *et al.* (1994) and Lee & Wyllie (1994) presented new data, and interpreted rounded calcite grains to be a solid phase and suggested that the revised interpretation of Kjarsgaard (in Macdonald *et al.*, 1993) was correct.

Subsequently, Lee & Wyllie (1997) studied six bulk composition along the albite–nepheline (Ne)–calcite join at 1·0 GPa and provided analyses of quenched conjugate liquids from seven experiments. Silicate (7·5–17·6 wt % Na_2O) and carbonate (16·0–40·2 wt % Na_2O) liquids have low to moderate alkali contents. Lee & Wyllie (1996, 1997*a*) importantly presented phase equilibria data and arguments that the round $CaCO_3$ globules in their experiments were a solid phase (as proposed by Lee & Wyllie, 1994). However, several studies on mantle xenoliths with rounded carbonate 'globules' have tended to ignore the interpretation of Lee & Wyllie (1994), and suggested instead that these carbonates represent melts of an immiscible origin (e.g. Chalot-Prat & Arnold, 1999; Kogarko *et al.*, 2001; Laurora *et al.*, 2001).

Based on previous experimental studies, it is clear that a re-examination of two-liquid ± calcite phase equilibria is required at variable P–T–X, including the minimum amount of alkalis required, if any, for silicate–carbonate immiscibility to occur at a given pressure and temperature. This would help to constrain the potential spatial association of carbonatite and silicate rocks in alkaline complexes, as well as the origin of carbonates in mantle xenoliths. In this study we have completely re-evaluated our previously published (Kjarsgaard & Hamilton, 1988, 1989*a*; Brooker & Hamilton, 1990) and unpublished (Kjarsgaard, 1990; Brooker, 1995) results, and present a complete characterization of the two-liquid field in P–T–X space at 0·1–2·5 GPa and 1225–1700°C. The data are presented using the 'traditional' quasi-ternary plot, projected from CO_2, with SiO_2 and Al_2O_3 combined at one apex; that is, the projection originally developed by Hamilton *et al.* (1979) to represent complex multi-component natural systems, and subsequently utilized by many workers to compare experimental data with natural compositions.

EXPERIMENTAL AND ANALYTICAL METHODS

Experimental methods

The majority of the experiments were carried out at Manchester University (MU), using an internally heated pressure vessel (IHPV) for experiments at 0·2 and 0·5 GPa or an end-loaded piston cylinder apparatus for the experiments at 1·5 GPa. Details of the IHPV techniques have been described by Kjarsgaard & Hamilton (1988, 1989*a*). The MU piston cylinder experiments utilized 19 mm talc–Pyrex assemblies with a tapered furnace (see Kushiro, 1976) and a Pt–Pt/Rh_{87} (S-type) thermocouple. Additional piston cylinder runs were also carried out at 1·0–2·5 GPa in a non end-loaded piston cylinder apparatus at Arizona State University (ASU) using 12 mm NaCl–Pyrex assemblies and a W/Re_5–W/Re_{26} (W-type) thermocouple. Further details for the ASU experimental methods have been provided by Brooker *et al.* (1998). A few additional experiments at 0·1–0·2 GPa (RB579, RB580, RB620) were performed in a rapid-quench TZM pressure vessel at the University of Bristol.

All reported piston cylinder pressures remain uncorrected for frictional effects, but this has been shown to be less than 3% for the talc–Pyrex assembly and negligible for the salt cells using the 'hot piston out' method (e.g. McDade *et al.*, 2002). However, comparison of results between the MU and ASU piston cylinder experiments suggests that the S-type thermocouple (MU) gave low readings at temperatures above 1200°C. Some of this may be caused by the high pressure dependence of the e.m.f. in S-type thermocouples (possibly requiring a 13°C correction at 1250°C and 1·5 GPa; Clark, 1959) compared with the negligible effect in the W-type. However, changes in the power requirements of the piston cylinder apparatus during runs suggest that a significant portion of the error is related to some time-dependent contamination of the Pt thermocouple, possibly from boron originating in the Pyrex parts of the assembly. To achieve internal consistency between the ASU and MU results, several experiments were repeated. Results from these experiments indicate that MU experiments at temperatures from 1175°C to 1200°C require correction by +25°C and experiments at temperatures from 1225 to 1325°C require correction by +50°C. All higher temperature experiments were performed at ASU and results for the melting point of calcite in the ASU apparatus (between 1510 and 1520°C at 1·5 GPa) are in excellent agreement with the data of Wyllie (1989). It should be noted that temperatures originally reported by Brooker & Hamilton (1990) were not subject to the temperature corrections noted above.

Starting materials for all experiments were silicate glasses (prepared from gels) and reagent grade Na_2CO_3 (Nc), $CaCO_3$ (Cc) and Al_2O_3 (Al). The nominal glass compositions (as confirmed by electron microprobe) are as follows, with ratios in wt % $SiO_2/Al_2O_3/CaO/Na_2O$; $R' = 69·5/19·7/10·8/0·0$; $E' = 63·1/12·8/24·1/0·0$; $An = 43·2/36·6/20·0/0·0$; $Ab = 68·7/19·4/0·0/11·8$; $2N = 38·1/20·0/0·0/41·9$. All starting materials were stored at 110°C and periodically dried at higher temperatures. Most of the silicate glasses (and hence the experiments) have an Al_2O_3/SiO_2 wt % ratio of 0·28 (equivalent to albite), although this ratio was varied up to 0·5 in some runs to cover the range found in typical alkali silicate extrusive rocks from carbonatite complexes. For piston cylinder experiments, starting mixes were weighed out, welded into 5 mm platinum capsules and loaded into the piston cylinder apparatus. Initially, 0·5 GPa of pressure was applied and the sample heated to 650°C, then temperature and pressure were increased in 0·1 GPa and 100°C steps to the required run conditions. The pressure was then overstepped and reduced (hot piston out). Piston cylinder experiments that showed evidence of blackening and carbon infiltration into the capsule were generally excluded from this study as the P_{CO2} may be lowered owing to the formation of CO and C from CO_2 (Brooker *et al.*, 1998). Runs were quenched isobarically and the recovered capsules examined for evidence of leakage during the run. Most fluid-saturated experiments gave an audible hiss on opening, but others did not. However, vesicles were usually present in the latter and results from these runs are consistent with fluid-saturated conditions. It is assumed that the fluid in these experiments was lost during or after the isobaric quench.

Analytical methods

Obtaining reliable quenched melt compositions was an important objective of this study. Analysis of volatile-rich, quenched carbonate and silicate melts is known to be a difficult problem. Thus considerable care was taken to ensure the reported compositions were as accurate as possible. Capsules were mounted in resin and polished to reveal the sample, using anhydrous lubricants. The composition of phases was determined by electron microprobe analysis (EMPA) using a Cameca Camebax electron microprobe at Manchester University for the majority of samples, and a Jeol 8600 JXA at Arizona State University for some additional experiments. The Cameca utilized an energy-dispersive spectrometer and a Link systems AN1000 computer running ZAF4 software. Accelerating potential was 15 kV and specimen current 3·0 nA. Standards employed were: Si, Ca (wollastonite); Al (corundum); Na (Amelia albite). The Jeol EMP used four wavelength-dispersive spectrometers and a Tracor computer with Bence–Albee reduction of raw data. Accelerating potential was 15kV and specimen current 10·0 nA. Standards employed were: Si, Ca (diopside); Al (corundum); Na (jadeite). On the Camebax a focused spot beam was rastered over a 100 μm square. This was found to be the minimum size required to record accurate Na

totals on synthetic quench carbonate melt standards on the Na_2CO_3–$CaCO_3$ join with >10 wt % Na_2O, and also some alkali-rich (but CO_2-free) silicate glass compositions prepared and utilized as internal standards. This minimum raster size may be related to the time taken for the beam to return to a given point and the migration time for Na to diffuse away from the beam, and then back to that position. The sizes of quench intergrowth textures and the distribution of any exsolved silicate spheres further dictate the size of the area for representative analysis of quenched carbonates. Similar results to the Cameca were obtained on the JEOL instrument utilizing a 50–100 μm defocused beam, with a short acquisition time for Na (15 s). It was noted that the use of an increasingly smaller raster area (Cameca) or a more tightly focused beam (JEOL) decreased the Na total whilst the other components show a proportional increase. This occurs up to the point where the total shows a dramatic decrease and permanent beam damage to the sample is apparent. A lower beam current can be used with less damage, but the inherent lower count rate requires a large number of analyses to obtain statistically accurate data. To some extent our method represents a compromise, as the opportunity for large raster analysis is limited by the quench texture and the variable quality of the polish. In some cases we have selected a few analyses as being the most representative of the carbonate liquid; in other cases the presented data are the average of up to 10 analyses. Silicate liquid analyses quoted in Tables 1–3 are the average of a minimum of five analyses. We have not reported errors or standard deviations in the data tables as some qualitative selection is involved (as discussed above) and data were acquired on different microprobes using different methods. However, for the majority of the data the deviation in the values used to create an average would plot within the size of the symbols in the quasi-ternary plots of this study. During the course of this study we were able to identify analyses with low totals by comparing shortfalls in microprobe data with the LECO CO_2 analyses (see below). In general 'bad' analyses with low totals tend to plot at lower Na_2O values.

CO_2 contents of selected silicate glasses were determined using a LECO C/S 300 analyser (see Brooker *et al.*, 2001, for details). For most samples, three aliquots were analysed and the results were all within 5% of the quoted values. LECO values were used to evaluate the validity and accuracy of using shortfalls from the electron microprobe analysis totals to estimate the CO_2 content by assuming that CO_2 is the only unanalysed component (note, however, that minor amounts of water, up to 0·5 wt %, have been identified by Fourier transform infrared spectroscopy in some run products). For silicate glasses the accuracy of the EMP shortfall method for CO_2 is ±10–20% (for silicate glasses with high CO_2 contents). The accuracy of this

Table 1: Experimental run conditions, starting compositions and run products in SAC + CO_2 (in wt %)

Run no.:	RB25	RB31	RB37	RB40	RB45	RB55	RB56	RB70	RB75	RB91	RB289	RB445	RB448	RB457	RB458	RB470	BK 70
T (°C):	1325	1325	1325	1325	1375	1325	1325	1275	1325	1375	1325	1400	1500	1435	1450	1435	1250
P (GPa):	1·5	1·5	1·5	1·5	1·5	1·5	1·5	1·5	1·5	1·5	1·5	1·5	1·5	1·5	1·5	1·5	0·5
Run duration (h):	3	10	2	3	18	21	29	20	17	4	20	5·5	0·75	1	1	4·5	12
Starting composition																	
	Cc70	Cc75	Cc60	Cc40	Cc60	Cc73	Cc78	Cc78	Cc78	Cc52	Cc*73	Cc*75	Cc*75	Cc*80	Cc*90	Cc*90	Cc85
	E′30	An25	R′40	R′60	R′40	E′27	R′22	R′22	R′22	R′48	E′27	E′25	E′25	E′20	E′10	E′10	An15
SiO_2	18·93	10·80	27·80	41·71	27·80	17·04	15·29	15·29	15·26	33·37	17·04	15·06	15·11	12·16	6·19	6·19	5·39
Al_2O_3	3·84	9·16	7·87	11·80	7·87	3·45	4·33	4·33	4·33	9·44	3·45	3·06	3·08	2·47	1·26	1·26	4·57
CaO	46·43	47·04	37·93	28·89	37·93	47·39	46·04	46·04	46·06	34·31	47·39	45·88	45·81	47·83	51·86	51·86	52·66
CO_2	30·80	33·00	26·40	17·60	26·40	32·12	34·32	34·32	34·32	22·88	32·12	36·00	35·99	37·54	40·69	40·69	37·41
Melt composition																	
SiO_2	39·90	29·61	37·27	41·53	30·50	39·75	39·36	43·09	39·55	n.a.	n.a.	24·64	15·30	13·18	6·23	11·68	26·93
Al_2O_3	8·44	19·61	11·27	12·10	9·38	9·62	11·72	12·17	11·85			5·06	3·26	2·72	1·33	2·52	27·22
CaO	41·32	41·24	41·91	32·59	43·24	41·94	40·10	36·43	41·67			47·70	51·00	51·51	53·65	52·02	42·46
Shortfall	10·34	9·54	9·55	13·78	16·88	8·69	8·82	8·31	6·93			22·60	30·44	32·59	38·79	33·78	3·39
Solid phases	Cc	Cc	Cc		QCc	Cc	Cc	Cc	Cc		Cc	Cc				Cc	Cc

Cc, calcite (see text for other starting materials); QCc, quench calcite in experiment; n.a., not analysed. Shortfall is the difference between the total of analysed components and 100%.
*Calcite cleavage rhombs included in starting material.

Table 2: Experimental run conditions, starting compositions and run products in SNAC + CO_2 at 0·1, 0·2, 0·5 and 1·5 GPa (in wt %)

	SNAC + CO_2 at 0·1 and 0·2 GPa													
Run no.:	RB580	RB579	BK129	BK34	BK23	BK17	BK130	BK3	RB620	BK18	RB84	RB86	BK5*	BK32
T (°C):	1250	1250	1250	1250	1250	1250	1250	1250	1250	1250	1225	1225	1250	1250
P (GPa):	0·1	0·1	0·2	0·2	0·2	0·2	0·2	0·2	0·2	0·2	0·2	0·2	0·2	0·2
Run duration (h):	1·5	1·5	30	2	1	2	30	3	2	2	6	6	2	2
Starting composition														
SiO_2	34·37	17·86	34·37	16·61	28·81	22·84	14·80	34·37	17·86	22·28	26·11	27·81	17·18	30·31
Al_2O_3	9·72	5·06	9·72	4·70	8·15	6·46	4·18	9·72	5·06	6·30	7·40	7·86	4·86	8·58
CaO	0·00	24·08	0·00	22·10	23·50	30·41	36·22	28·04	24·08	29·65	34·72	34·57	42·06	24·7
Na_2O	35·15	21·21	35·15	24·16	14·42	11·27	10·66	5·91	21·21	12·43	4·50	3·51	2·96	12·11
CO_2	20·76	31·79	20·76	32·46	25·15	29·05	34·16	21·99	31·79	29·33	27·27	26·25	32·94*	24·3
Silicate liquid														
SiO_2	52·15	41·74	52·05	50·64	41·96	34·08	30·97	42·54	48·59	35·61	32·5	33·01	28·55	36·46
Al_2O_3	15·62	13·21	15·11	14·40	12·83	11·42	9·91	11·81	14·05	10·02	9·51	10·19	3·67	10·38
CaO	0·00	23·17	0·00	14·62	21·82	35·31	38·48	34·56	17·59	30·41	46·25	45·02	48·12	29·13
Na_2O	31·12	18·87	27·00	19·03	14·52	11·30	11·14	7·33	17·08	11·44	5·8	4·78	5·81	13·85
Shortfall	1·11	3·01	5·84	1·31	8·87	7·90	9·50	3·77	2·69	12·52	5·94	7	13·87	10·18
CO_2 by LECO								3·87	2·50		8·6	7·81		8·53
Carbonate liquid														
SiO_2	1·08	6·96	0·51	3·90	6·52	9·63	15·47	No CL	4·80	9·43	No CL	No CL	No CL	No CL
Al_2O_3	0·07	0·80	0·17	0·50	0·70	0·90	1·37		0·60	0·80				
CaO	0·00	28·65	0·00	28·10	34·03	36·84	39·41		30·08	38·33				
Na_2O	42·20	25·49	53·29	28·54	20·59	12·88	10·66		25·56	15·82				
Shortfall	56·66	38·10	46·03	38·96	38·16	39·74	33·09		38·96	35·62				
Starting mix														
Cc		43·00		39·41	41·91	54·22	64·59	50·00	43·00	52·88	62·00	54·00	75·00*	44·11
Ab	50·00	26·00	50·00	24·16	41·91	33·23	21·53	50·00	26·00	32·41	38·00		25·00*	44·11
Nc	50·00	31·00	50·00	36·43	16·18	12·55	13·88		31·00	14·71		6·00		11·78
R′												40		

(continued)

Table 2: Continued

	SNAC + CO_2 at 0·5 GPa																				
Run no.:	BK58	BK73	BK42	BK27	BK21	BK25	BK49	BK48	BK20	BK43	BK9	BK10	BK12	BK66†	BK16	BK114	BK115	BK116	BK117	BK112	BK113
T (°C):	1250	1250	1250	1250	1250	1250	1250	1250	1250	1250	1250	1250	1250	1250	1250	1250	1250	1250	1250	1250	1250
P (GPa):	0·5	0·5	0·5	0·5	0·5	0·5	0·5	0·5	0·5	0·5	0·5	0·5	0·5	0·5	0·5	0·5	0·5	0·5	0·5	0·5	0·5
Run duration (h):	26	12	26	3	4	3	4	4	4	6	3	3	3	12	4	12	12	12	12	12	12
Starting composition																					
SiO_2	34·37	10·18	10·81	13·31	21·04	23·77	14·29	15·53	32·15	20·70	34·37	26·12	51·56	17·19	44·19	32·93	26·11	43·55	36·56	59·63	49·71
Al_2O_3	9·72	2·88	3·06	3·76	5·95	6·72	4·04	4·39	9·09	5·85	9·72	7·39	14·58	4·86	12·49	9·31	7·39	12·31	10·34	16·86	14·08
CaO	0·00	18·17	26·46	32·58	28·01	31·64	34·98	38·00	3·63	35·88	28·04	34·77	14·02	42·06	12·02	26·86	34·72	16·72	21·16		6·05
Na_2O	35·15	32·62	23·54	15·47	14·99	9·35	12·31	8·32	32·87	7·01	5·91	4·49	8·86	2·95	15·96	8·12	4·50	11·48	11·60	18·00	18·41
CO_2	20·76	36·16	36·15	34·90	30·04	28·54	34·42	33·80	22·26	30·59	21·99	27·26	10·99	32·98	15·36	22·81	27·28	15·95	20·36	5·51	11·75
Silicate liquid																					
SiO_2	55·48	50·94	46·14	39·89	42·14	31·81	33·91	28·57	53·99	25·06	41·43	34·44	56·11	31·77	50·79	39·92	33·88	49·56	42·58	63·53	n.a.
Al_2O_3	16·31	17·56	18·32	16·50	17·06	10·10	15·54	8·90	17·12	7·07	11·78	9·46	15·65	9·01	14·47	11·30	9·63	14·19	12·07	17·54	assumed
CaO	0·00	7·20	14·73	25·29	20·66	36·57	30·34	39·44	2·59	42·31	33·46	39·10	15·29	41·79	14·01	31·82	38·91	20·08	23·88		as
Na_2O	26·49	21·60	17·99	12·42	14·14	9·85	10·80	9·14	24·31	8·34	6·91	6·52	9·50	5·80	18·04	10·06	5·90	13·33	13·76	18·32	above
Shortfall	1·72	2·70	2·81	5·90	6·00	11·67	9·41	13·94	2·00	17·22	6·42	10·48	3·45	11·62	2·69	6·90	11·68	2·84	7·71	0·61	
CO_2 by LECO					3·1				0·82	16·56	6·29		0·95	10·74†	3·91		11·47	3·79	7·95	0·66	0·80
Carbonate liquid																					
SiO_2	0·31	1·14	3·53	6·24	5·56	10·38	7·65	13·03	0·81	No	No	No	No	No	No	No	No	No	No	No	No
Al_2O_3	0·31	0·26	0·40	0·60	0·46	1·41	0·91	2·34	0·33	CL	CL	CL	CL	CL	CL	CL	CL	CL	CL	CL	CL
CaO		22·16	30·35	37·37	35·80	42·03	40·52	40·70	4·07												
Na_2O	52·73	32·64	25·46	17·19	19·81	11·62	14·41	8·36	48·96												
Shortfall	46·65	43·80	40·26	38·60	38·37	34·56	36·52	35·57	45·83												
Starting mix																					
Cc		32·39	47·19	58·09	49·94	56·42	62·37	67·76	6·48	63·99	50·00	62·00	25·00	75·00	21·42	47·90	62·00	29·81	37·73		10·81
Ab	50·00	14·81	15·73	19·36	30·61	34·58	20·79	22·59	46·76	30·11	50·00	38·00	75·00	25·00	64·27	47·90	38·00	63·35	53·18	86·74	72·35
Nc	50·00	52·79	37·08	22·54	19·46	9·00	16·84	9·66	46·76	5·90					14·30	4·20		6·83	9·09	13·26	14·84

(continued)

Table 2: Continued

	SNAC + CO_2 at 1·5 GPa																	
Run no.:	RB8	RB10	RB26	RB27	RB30	RB34	RB36	RB63	RB66	RB74	RB88	RB99	RB100	RB111	RB112	RB106	RB107	RB108
T (°C):	1350	1275	1275	1225	1325	1275	1325	1275	1275	1225	1275	1275	1275	1275	1275	1325	1325	1325
P (GPa):	1·5	1·5	1·5	1·5	1·5	1·5	1·5	1·5	1·5	1·5	1·5	1·5	1·5	1·5	1·5	1·5	1·5	1·5
Run duration (h):	3	3	5	5	4	3	6	20	24	5	7	27	37	13	24	5	7	23
Starting composition																		
SiO_2	26·11	26·11	19·05	19·05	19·05	21·30	21·30	27·81	19·00	27·81	44·66	15·11	17·86	16·15	16·49	15·80	13·05	9·96
Al_2O_3	7·40	7·40	5·40	5·40	5·40	6·04	6·04	7·86	10·00	7·86	12·65	4·28	5·06	6·57	6·67	4·48	3·70	2·82
CaO	34·72	34·72	25·33	25·33	25·33	28·33	28·33	34·57		34·57		29·12	24·08	22·68	11·20	19·60	16·80	12·88
Na_2O	4·50	4·50	19·09	19·09	19·09	14·43	14·43	3·51	50·24	3·51	28·16	17·81	21·21	22·67	34·42	27·29	32·08	38·27
CO_2	27·27	27·27	31·13	31·13	31·13	29·90	29·90	26·25	20·76	26·25	14·53	33·68	31·79	31·93	31·22	32·83	34·37	36·07
Silicate liquid																		
SiO_2	30·80	42·05	57·66	60·14	53·39	53·85	51·18	29·80	35·40	33·14	61·00	57·00	58·65	55·09	54·58	55·59	55·63	58·59
Al_2O_3	8·70	11·56	17·50	17·93	15·49	16·64	15·74	9·10	21·70	10·15	17·50	17·13	17·84	23·13	21·92	16·79	16·68	17·30
CaO	38·00	32·22	8·19	5·22	12·88	13·71	16·50	40·40		37·20		9·90	6·50	3·98	1·52	7·04	4·96	2·54
Na_2O	4·70	5·39	16·19	14·91	15·94	13·68	14·08	4·20	37·70	4·85	20·20	15·17	16·64	17·80	20·80	19·19	20·66	21·34
Shortfall	17·80	8·78	0·46	1·80	2·30	2·12	2·50	16·50	5·20	14·66	1·30	0·80	0·37	0·00	1·18	1·39	2·07	0·23
CO_2 by LECO	15·58	<11·44‡						15·91	4·29		2·84	2·78	2·93	2·76	2·30	3·52	2·50	2·45
Carbonate liquid																		
SiO_2	No CL	10·18	1·43	0·69	3·00	2·65	5·64	No CL	5·00	No CL	0·80	2·16	1·53	0·79	0·95	1·90	1·50	1·28
Al_2O_3		1·24	0·26	0·17	0·51	0·25	0·80		0·30		0·30	0·30	0·23	0·18	0·20	0·28	0·13	0·24
CaO		47·38	35·74	36·78	33·97	39·32	38·56					36·86	32·70	31·78	14·72	25·88	21·12	15·52
Na_2O		6·49	19·72	19·83	20·73	16·44	16·82		56·40		44·70	18·91	22·34	24·32	35·47	28·01	32·13	36·29
Shortfall		34·71	42·85	42·53	41·79	41·34	38·18		38·30		54·20	41·77	43·20	42·93	48·27	43·93	45·12	46·67
Starting mix (wt %)																		
Cc	62·0	62·0	45·30	45·30	45·00	50·60	50·60	54·00		54·00		52·00	43·00	40·50	20·00	35·00	30·00	23·00
Ab	38·0	38·0	27·70	27·70	28·00	31·00	31·00				65·00	22·00	26·00	23·50	24·00	23·00	19·00	14·50
Nc			27·00	27·00	27·00	18·40	18·40	6·00	50·00	6·00	35·00	26·00	31·00	34·00	54·00	42·00	51·00	62·50
R′								40·00		40·00								
Other									50N2					$2Al_2O_3$	$2Al_2O_3$			

LECO is a trade name for the bulk carbon analyser. It should be noted that RB579 and RB620 are the same RB100 starting composition as in Table 3. Starting materials are described in the text. No CL, no carbonate liquid present.

*BK5 starting mix has ~9 wt % silver oxalate added (additional CO_2 to listed amount) and run products include calcite and melilite.

†BK66 has 33 wt % calcite (as determined by mass balance). The LECO CO_2 result for this silicate glass was 25·4 wt %, but this has been corrected to account for the calcite.

‡LECO data for RB10 ranged from 9·9 to 11·44 wt % possibly as a result of inclusion of Cc in some aliquots. Cc was a stable phase in RB10, RB63 and RB74.

Table 3: Experimental run conditions and run products using the RB100 bulk composition (in wt %)*

Run no.:	RB100a	RB100c	RB100f	RB100b	RB100d	RB100e	RB100g	RB100i	RB100h	RB100i	RB100k	RB100m	RB100n	RB100o	RB100p	RB100j	RB100l
T (°C):	1300	1300	1300	1550	1600	1425	1300	1575	1700	1575	1275	1275	1300	1300	1300	1275	1275
P (GPa):	2·5	2·0	1·0	1·5	1·5	1·5	1·5	1·5	1·5	1·5	1·5	1·5	1·5	1·5	1·5	1·5	1·5
Run duration (h):	17	6	2·5	1·25	0·75	1·50	4·00	1	0·25	1	2·5	5	2	3	3	5	6
Loaded CO_2	31·79	31·79	31·79	31·79	31·79	31·79	31·79	31·79	31·79	31·79	22·03	24·79	24·79	22·03	19·80	15·78	11·00
Silicate liquid																	
SiO_2	59·30	58·50	52·36	41·15	38·19	49·00	55·90	41·42	40·79	41·42	26·52	37·98	38·29	25·40	23·36	n.a.†	n.a.†
Al_2O_3	17·43	17·51	16·65	13·65	13·06	15·66	17·57	13·94	13·47	13·94	9·08	12·82	12·62	8·16	7·34		
CaO	3·10	4·09	9·84	16·71	18·2	11·64	6·94	17·32	17·71	17·32	26·01	20·82	20·66	26·81	28·26		
Na_2O	16·09	16·38	17·52	18·35	18·54	17·42	16·90	17·91	18·21	17·91	21·44	18·84	18·38	21·59	22·40		
Shortfall	4·08	3·52	3·62	10·14	12·1	6·28	2·69‡	9·41	9·81	9·41	16·95	9·54	10·05	18·04	18·61		
Carbonate liquid																	
SiO_2	0·75	0·87	2·27	7·69	7·9	3·38	1·39	7·48	9·11	7·48	14·59	6·96	8·06	16·30	15·65	n.a.	No CL
Al_2O_3	0·22	0·14	0·13	1·6	1·71	0·42	0·10	1·45	1·97	1·45	3·29	0·81	1·13	4·11	3·91		
CaO	31·82	31·18	30·58	27·35	27·75	29·57	32·46	28·93	29·80	28·93	27·57	28·71	29·43	27·94	27·57		
Na_2O	22·34	24·07	24·88	25·47	24·88	24·63	23·52	24·09	23·19	24·09	25·44	25·85	24·64	24·62	25·94		
Shortfall	44·86	43·75	42·14	37·9	37·77	42·00	42·54	38·05	35·93	38·05	29·12	37·67	36·74	27·03	26·93		

*All starting composition same as RB100 in Table 2 except for runs with loaded $CO_2 < 31·79$. For these experiments the other components are in same proportions as RB100 (see text for details).
†Unidentified crystal phases also present.
‡LECO = 3·05 wt % CO_2.

method falls to ±50% with low CO_2 contents (usually higher SiO_2, more polymerized compositions). Application of the microprobe shortfall method for carbonate liquids from the experiments also appears to be valid, as the stoichiometric CO_2 content for quenched melts on the Na_2CO_3–$CaCO_3$ join is reproduced. Finally, it should be noted that poor quality surface polish appears unavoidable for some quenched melts, and this always results in unrealistically high probe shortfalls.

RESULTS

Immiscible liquid textures of run products

Photomicrographs from selected runs are used to illustrate some definitive textures in Figs 1–3. Experiments with high- to moderate-Na_2O bulk compositions typically contained a silicate glass bead, surrounded by quenched carbonate melt (Fig. 1a). The characteristic quench textures seen in our two-liquid experiments are similar to those observed in previous studies (e.g. Koster van Groos & Wyllie, 1966; Freestone & Hamilton, 1980), and are interpreted as representing two immiscible liquids at run conditions. When there is closure of the solvus owing to higher temperature, lower pressure, low alkali content, or CO_2 undersaturation, the compositions and physical properties of the two liquids become increasingly similar. Hence separation of the two liquids is typically less distinct, as shown in Fig. 1b (see also Brooker, 1998, fig. 2e).

The quench texture of the carbonate liquids varies between parallel lamellar patterns (Figs 1a and 2), to more random amoeboid-like to dendritic textures (e.g. Fig. 3b). Spheres of silicate liquid of variable size are commonly observed in moderate- to low-alkali quenched carbonate liquids. Occasionally, carbonate spheres are seen in the silicate bead (Fig. 2). It is important to determine which of these spheres have exsolved from their host liquid during quenching and therefore represent a constituent part of that original equilibrium liquid composition, and spheres that represent the equilibrium conjugate liquid. Typically a bimodal distribution of sphere sizes is observed. The largest sized spheres represent liquid that has failed to coalesce with the main body of liquid at run conditions (e.g. sphere SL2 in Fig. 2).

For experiments in the IHPV, which has a slower quenching rate than experiments run in a piston cylinder apparatus, small, non-equilibrium, quench, exsolved spheres are common. It should be noted that the low $SiO_2 + Al_2O_3$ contents of some low-alkali carbonate liquid analyses of Kjarsgaard & Hamilton (1988, 1989*a*) were generated by subtracting a silicate melt component that was thought to represent non-coalesced 'equilibrium' silicate spherules. However, Kjarsgaard (1990) reassessed the original microprobe data and noted two distinct

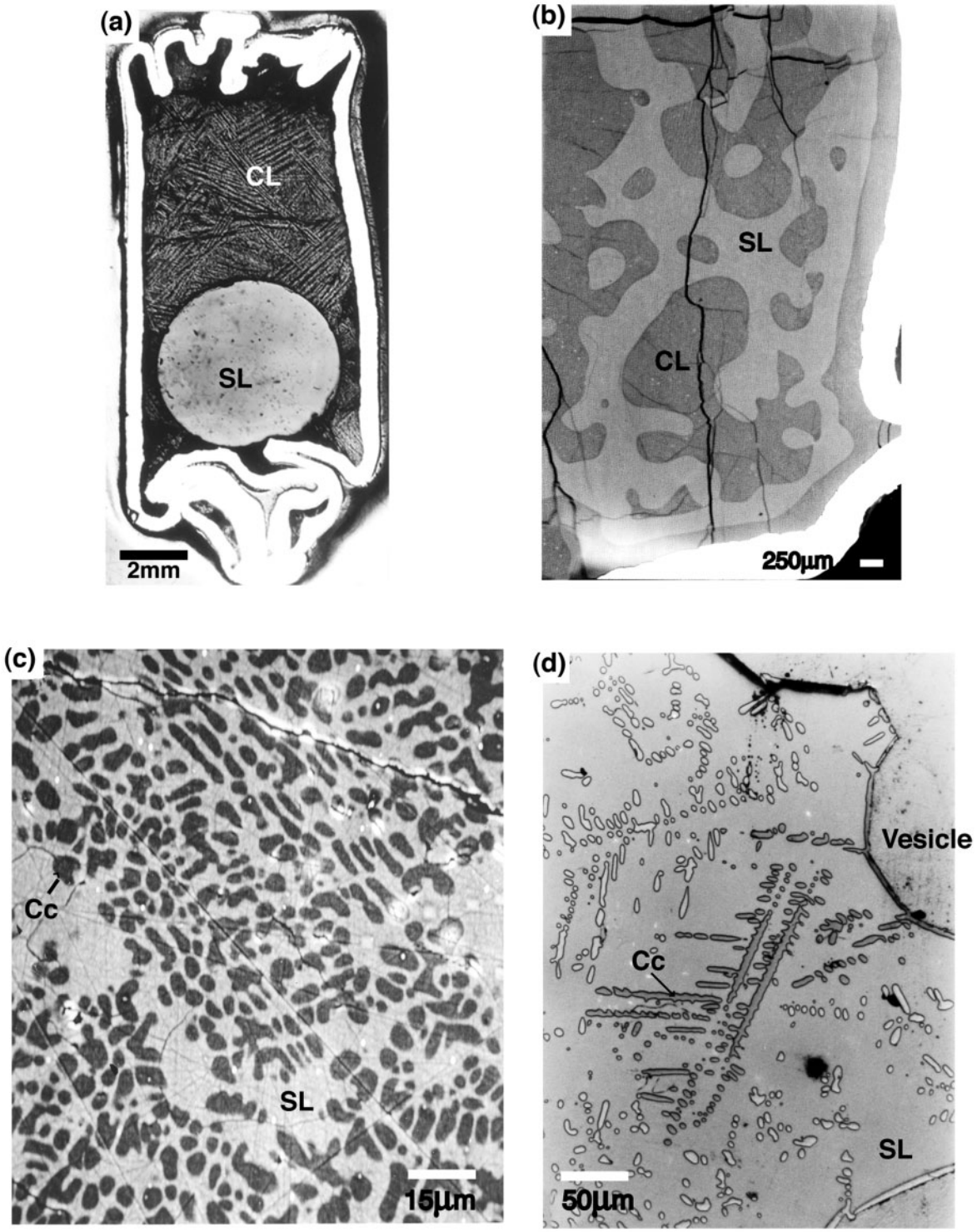

Fig. 1. Reflected light photomicrographs (RLP) and backscattered electron (BSE) images of immiscible silicate and carbonate liquids and 'globular' calcite textures. (a) A typical two-liquid texture with a silicate bead (SL) at the base of the capsule surrounded by a quench intergrowth of carbonate liquid (CL). RLP, experiment RB100 ($P = 1{\cdot}5$ GPa, $T = 1275^{\circ}$C). This sample has been etched with acid to enhance the carbonate quench texture. (b) illustrates the non-spherical texture produced by two immiscible liquids with similar compositions, resulting in the silicate (SL) and carbonate (CL) liquids forming blobs and inter-penetrative tubes. BSE image, experiment RB100o ($P = 1{\cdot}5$ GPa, $T = 1300^{\circ}$C). (c) $CaCO_3$ (Cc) 'globules' in silicate liquid (SL) appear to show deformation and coalescence textures similar to those in (b), albeit at a different scale. BSE image, experiment BK66 ($P = 0{\cdot}5$ GPa, $T = 1250^{\circ}$C). (d) The calcite (Cc) 'globules' in silicate liquid (SL) are characterized by a defined complex structure. RLP, experiment RB37 ($P = 1{\cdot}5$ GPa, $T = 1325^{\circ}$C).

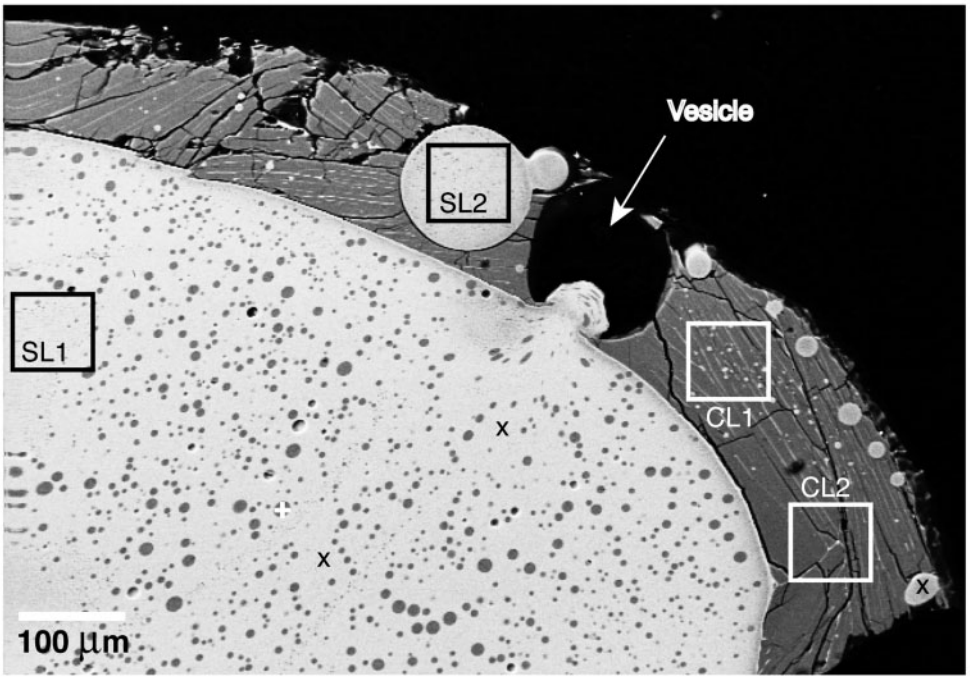

Fig. 2. BSE image of stable and quench exsolution textures, experiment RB579 ($P = 0{\cdot}1$ GPa; $T = 1250°$C). It should be noted that both the main silicate bead and the quench carbonate liquid have populations of small spheres. The carbonate liquid contains very small aluminosilicate spheres that are exsolved during the quench (areas CL1, CL2). The exsolution in the carbonate liquid is particularly heterogeneous but analyses for the two squares marked CL1 and CL2 produce similar results (i.e. equivalent Si–Al contents). These small spheres are distinct from the larger, uncoalesced silicate spheres (e.g. area SL2), which tend to occur near the capsule wall, and have not coalesced with the main silicate bead. Analysis of the silicate areas SL1 and SL2 produced similar results.

populations of silicate spheres: those $>\sim$15 μm had similar composition to the main silicate bead, whereas spheres $<\sim$15 μm were more silica- and alumina-rich, with compositions more appropriate to a lower temperature silicate solvus (i.e. these silicate spheres were exsolved from the carbonate liquid during the slow quench of the IHPV). The analyses for the 0·2 and 0·5 GPa samples of Kjarsgaard & Hamilton (1988, 1989*a*) that are presented in this study are either the original raw microprobe data (without the silicate component subtracted) or new analyses. These revised and new data presented in this paper supersede all previously published values.

Solid $CaCO_3$ 'globules'

The original interpretation of silicate–carbonate liquid immiscibility for very low-Na_2O and Na_2O-free bulk compositions (Kjarsgaard & Hamilton, 1988, 1989*a*) was based on the presence of rounded 'globules' or spheres of near pure $CaCO_3$ composition. These globules appeared to show coalescing textures (e.g. Fig. 1c). Increasing the run time did not change the texture, as might be expected for coalescence, but then neither would the intermingling immiscible textures shown in Fig. 1b. Although the texture in Fig. 1c does show similarities to the intermingling immiscible liquids in Fig. 1b (albeit of a different size scale), they are similar to the equilibrium calcite crystal morphology as illustrated in Fig. 1d.

'Three-liquid' textures observed in the experiments of Brooker & Hamilton (1990) included: (1) an 'apparent' curved meniscus between $CaCO_3$ and two other liquids (Fig. 3a and b); (2) similar round spheres of silicate liquid in both the $CaCO_3$ phase and quenched Ca–Na carbonate liquid (Fig. 3b); (3) apparent vesiculation in the $CaCO_3$ (Fig. 3a). Experiments with calcite rhombs added to low-Na_2O bulk composition starting mixes did not retain these crystals during the run, giving the impression that they had melted (e.g. Fig. 3a). Alkali-free runs at 1·5 GPa appear to show 'coalescing' and 'deforming' $CaCO_3$ 'globules' (Fig. 3c; see also Kjarsgaard & Hamilton, 1989*a*, fig. 15.5). Collectively, these textures were taken to indicate a liquid state for the 'globular' $CaCO_3$ phase.

To constrain the nature of the 'globular' $CaCO_3$ phase, new experiments in the Na_2O-free system ($SAC + CO_2$) were undertaken at 1·5 GPa and variable temperature. The bulk compositions utilized and resultant silicate liquid compositions are reported in Table 1 and Fig. 4. The liquidus is well constrained, and in Fig. 4 this projects to the melting point of pure calcite under CO_2-saturated conditions. The very low $SiO_2 + Al_2O_3$ content ($<$0·5 wt %) of the $CaCO_3$ phase in all experiments is a consistent

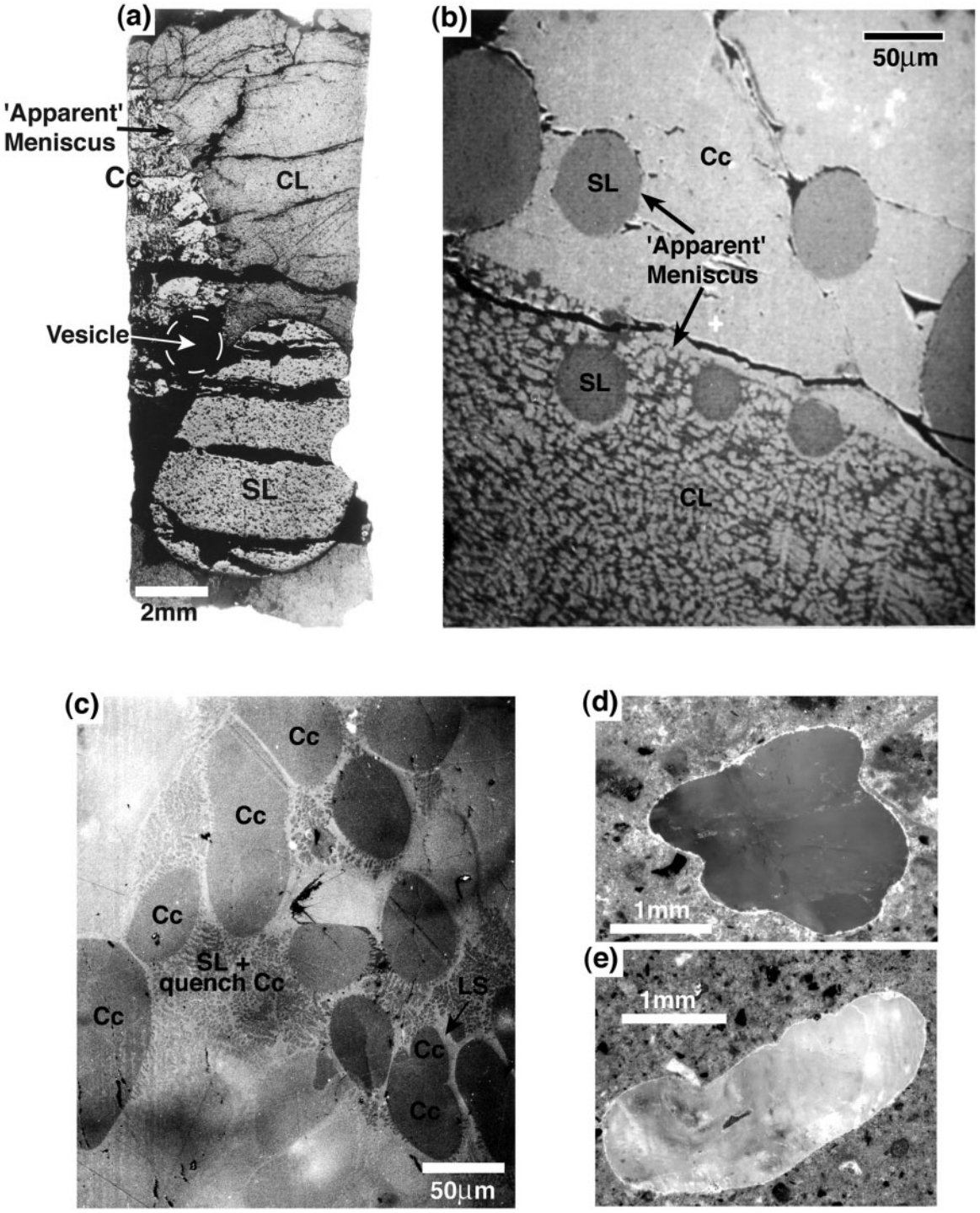

Fig. 3. Characteristic textures for $CaCO_3$ grown in the experiments of Brooker & Hamilton (1990). (a) Silicate (SL) and carbonate (CL) immiscible liquids are similar to those shown in Fig. 1a, but this experiment also contains a large $CaCO_3$ (Cc) phase with a vapour bubble (vesicle) and an 'apparent' meniscus. A single calcite cleavage fragment that was included in the starting mix is no longer apparent. Experiment RB130, $P = 1{\cdot}5$ GPa, $T = 1275°C$. (b) Round silicate spheres are found in both the quenched Na–Ca carbonate liquid (CL) and the $CaCO_3$ 'globules'. BSE image, experiment RB130. (c) Small $CaCO_3$ (Cc) 'globules' appear to deform larger ones, whereas similar-sized 'globules' appear to deform each other equally before 'coalescing', consistent with relative differences in surface tension. Also noteworthy is the very fine-grained interstitial quench calcite associated with the silicate glass (SL). BSE image, experiment RB104, $P = 1{\cdot}5$ GPa, $T = 1275°C$. In (d) and (e) similar 'globular'-shaped high-Sr, Ba magmatic calcite crystals are imaged in a nephelinite tuff from Shombole volcano, East African Rift (sample kindly supplied by M. Le Bas).

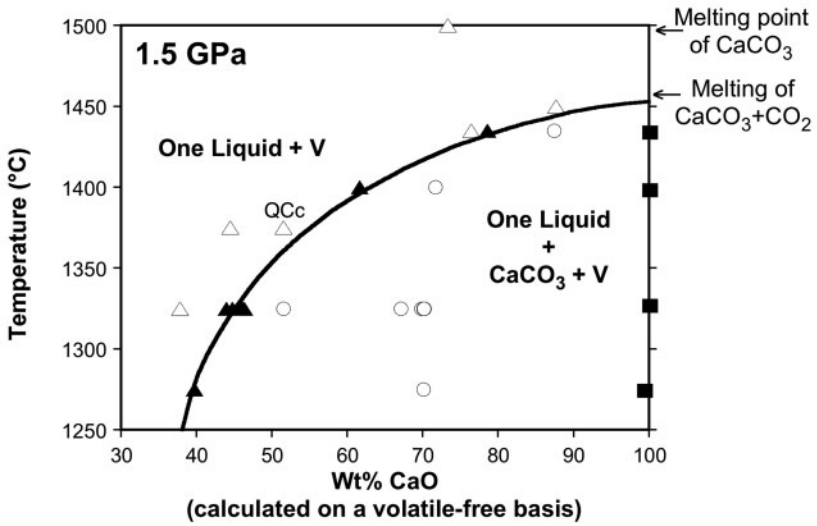

Fig. 4. *T–X* diagram for experiments along the Na_2O-free join ($SiO_2 + Al_2O_3$)–CaO. Circles are starting compositions; filled triangles are the liquids in equilibrium with an almost pure $CaCO_3$ phase (squares). Open triangles are single-liquid experiments. Open triangle QCc is a run that contained dendritic quench calcite. The melting points for calcite and calcite plus excess CO_2 are from Wyllie (1989). It should be noted that a range of bulk Al_2O_3/SiO_2 wt % ratios are represented (0·2–0·85).

feature. There is no liquid immiscibility, nor an inflection of the liquidus to indicate an increased solubility of SiO_2 and Al_2O_3 in the 'globular' $CaCO_3$ phase, as would be expected on approaching the high-temperature consolute point of a two-liquid solvus.

In some alkali-free experiments there is evidence of a 'structure' developed by the $CaCO_3$ phase (Fig. 1d). This dendritic 'Christmas tree' crystallization pattern is distinct from the quench carbonate liquid textures observed in other experiments. A much more random dendritic pattern is observed in quench carbonate liquids (Fig. 3b). The RB37 run products (Fig. 1d) with 'Christmas tree' calcite grains represent a stable calcite solid phase, based on the phase relations illustrated in Fig. 4. Jago & Gittins (1991) showed a similar morphology for calcite grown at atmospheric pressure. The tabular to dendritic calcite textures described here are also observed in hypabyssal kimberlites (e.g. Dawson & Hawthorne, 1973; Mitchell, 1997).

A range of textures between the isolated calcite 'globules' in Fig. 1c and the more complex patterns in Fig. 1d are observed. The initial development of these structures, coupled with the subsequent (variable) quench rate, produces calcite crystals with the appearance of 'coalescence' and 'liquid-like' forms. The rounded 'globular' form of calcite crystals has been produced in numerous experimental studies (e.g. Wyllie & Tuttle, 1960; Maaloe & Wyllie, 1975). Experiments on a natural nephelinite composition (see Kjarsgaard, 1998, fig. 1c) produced globular calcite in equilibrium with two liquids and clinopyroxene. Examples of some large natural magmatic (high-Sr, Ba) calcite crystals that have this 'globular' form are illustrated in Fig. 3d and e. These are set in an lithic tuff surrounded by ash rather than liquid.

A further experiment designed to illustrate the '*in situ*' stability of $CaCO_3$ utilized an Na_2O-free bulk composition, with $CaCO_3$ added both as a fine powder (introduced as a layer across the charge) and as calcite cleavage rhombs (see Table 1). The outlines of the original calcite rhombs are still present and show no evidence of melting (Fig. 5a), whereas the silicate liquid contains numerous small $CaCO_3$ 'globules' (Fig. 5b). In addition, the thin layer of calcite powder placed across the centre of the charge remained a single layer during the run, again with no evidence of melting (Fig. 5b). It should be noted that the large calcite rhombs observed in this experiment are no longer single crystals, but a mosaic of disoriented calcite crystals (Calcite I as confirmed by X-ray diffraction), with curvilinear internal boundaries. The observation of Calcite I is consistent with the inversion of high temperature–pressure calcite IV or V polymorph (see Carlson, 1983) during quenching. It is unclear why the original calcite rhombs are retained in these alkali-free experiments but were dissolved and redistributed in the Na_2O-bearing experiments of Brooker & Hamilton (1990; Fig. 3a). This may be related to the presence of a Na–Ca-carbonate liquid in the latter experiments and the minimization of interfacial energy to give a single boundary reminiscent of an immiscible contact (e.g. Fig. 3a and b).

Natural examples of mosaic-textured calcite crystals that have similar textures to those of the experiments are illustrated in Fig. 5c and d. These textures are also observed for some carbonates in mantle xenoliths (Ionov *et al.*, 1993,

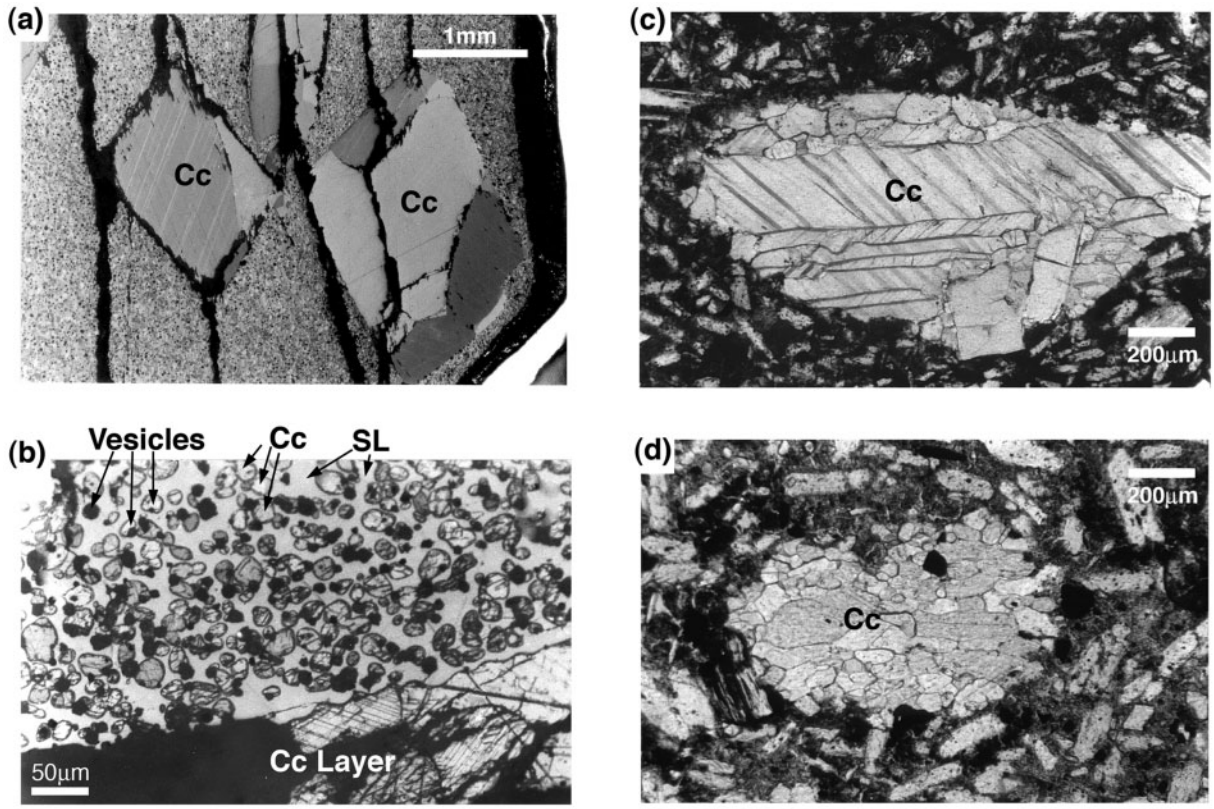

Fig. 5. Calcite rhomb and calcite aggregate textures from experiments and natural samples. (a) Several large calcite aggregates (with rhombic outlines) can be seen; these are remnants of cleavage fragments added to the starting mix. This definitively illustrates that calcite remains a solid phase in this run. RLP, experiment RB289 ($P = 1{\cdot}5$ GPa, $T = 1325^{\circ}$C). (b) Detail of (a) illustrating the rounded calcite (Cc) 'globules' in silicate liquid (SL), and the remnant intact thin layer of calcite (partly plucked out) in this run. RLP, with sample acid etched. (c) and (d) show rapidly quenched calcite phenocrysts from a carbonatite dyke (Brettel, Kaiserstuhl) that shows the same 'aggregate' texture as in (a). RLP.

1996; Ionov, 1998). Mosaic-textured calcite in some carbonatite lavas has been interpreted as evidence of calcite pseudomorphs replacing various other phases such as nyerereite (e.g. Deans & Roberts, 1984). Although this mechanism may be true for some examples, it is clear that this texture could also be produced by inversion of a metastable high temperature–pressure calcite polymorph as suggested by Keller (1989), Barker & Nixon (1989) and Jago & Gittins (1991).

Characteristics of the silicate–carbonate two-liquid field

The solvus in P–T *space*

The interpretation of the $CaCO_3$ 'globule' phase as solid calcite crystals allows us to refine and redefine the two-liquid field for the SNAC + CO_2 system at variable P–T conditions. The silicate and carbonate liquid compositions that define the two-liquid field at 0·1, 0·2 and 0·5 GPa at 1250°C and at 1·5 GPa and 1275°C are listed in Table 2 and plotted in Fig. 6a–c. Data for single silicate liquid (±calcite and other silicate solid phases) experiments are included on these diagrams, as they provide important constraints in defining the extent of the two-liquid field (although caution is required very close to the solvus; see above). Excess CO_2 fluid was present in all these runs, hence P_{CO2} is assumed to be equal to P_{total}. It should be noted that the tie-lines between conjugate liquids in these figures tend to pass slightly below the starting bulk compositions, the offset increasing with loaded bulk Na_2O content (and possibly pressure). This is the expected consequence of an Na_2O-rich component dissolved in the coexisting fluid phase, as previously documented by Koster van Groos & Wyllie (1973), Verwoerd (1978), Seifert *et al.* (1979), Wendlandt & Harrison (1979) and Freestone & Hamilton (1980), but can also arise as an analytical artefact (alkali loss during microprobe analysis).

Starting compositions for the 0·1, 0·2 and 0·5 GPa two-liquid experiments have the same Al_2O_3/SiO_2 ratio as albite (0·28 in wt %). In the 1·5 GPa experiments samples RB111 and RB112 (dashed tie-lines in Fig. 6c) and some of the experiments of Brooker & Hamilton (1990) Al_2O_3/SiO_2 wt % ratios range from ≥0·28 to 0·5. There is no apparent effect on the solvus topology for this range of Al_2O_3/SiO_2 ratios, although there are considerable

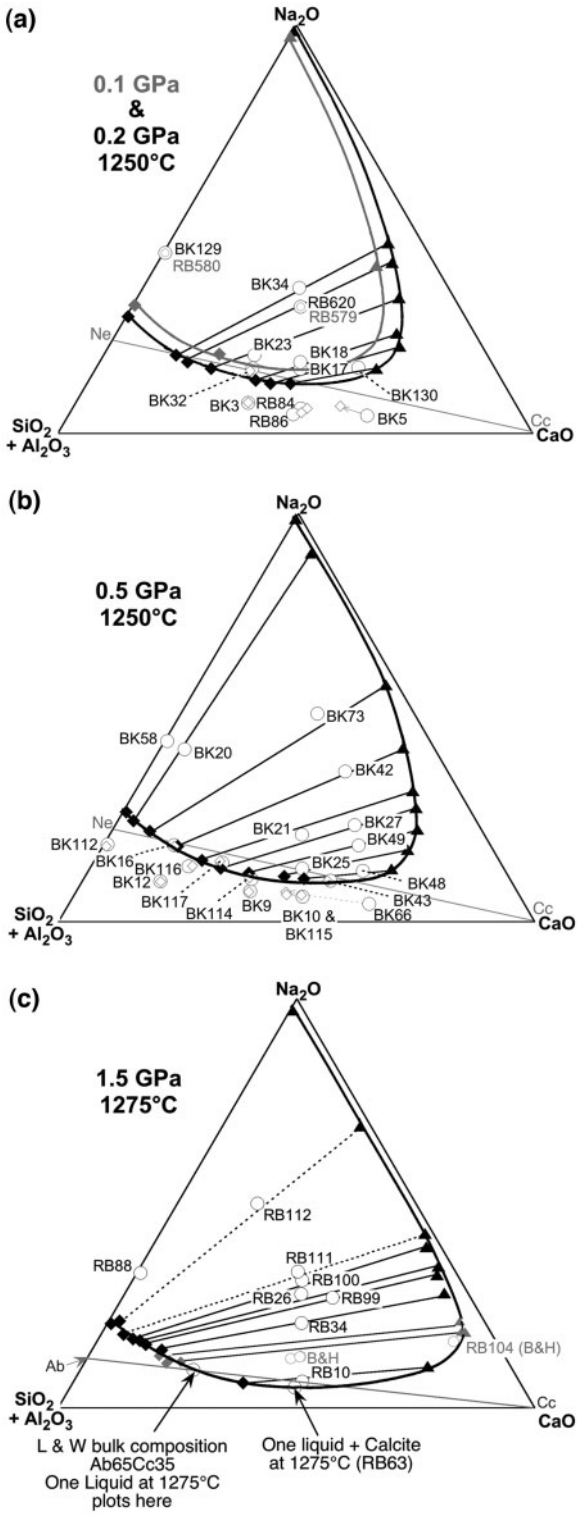

Fig. 6. The extent of the silicate–carbonate miscibility gap as plotted on quasi-ternary plots projected from CO_2. Conjugate silicate and carbonate liquids are joined by tie-lines. Starting (bulk) compositions are open circles, immiscible silicate liquids are filled diamonds, immiscible carbonate liquids are filled triangles and single-liquid experiments are open diamonds. It should be noted that several single-liquid runs are within the two-liquid solvus (see text). (a) 0·1 and 0·2 GPa, 1250°C (except RB84 and RB86 at 1225°C). Grey symbols are the 0·1 GPa data. The grey arrow from the BK5 starting composition to the silicate liquid represents the effect of crystallizing 16 wt % melilite, as estimated by mass balance. It should be noted that the bulk composition for RB579 and RB620 is the same as RB100 in (c). (b) 0·5 GPa, 1250°C, (c) 1·5 GPa, 1275°C; 1·5 GPa data in grey are from Brooker & Hamilton (1990); bulk compositions RB110, 126 and 130 are from that study, as well as RB104, although the temperature has been adjusted from the reported value of 1225°C (see text for details). The dotted tie-lines are for runs with bulk wt % Al_2O_3/SiO_2 of 0·4–0·45 (all other runs have $Al_2O_3/SiO_2 = 0·28$). The position of the nepheline (Ne) – calcite (Cc) join in a and b, and the albite (Ab) – calcite (Cc) join in c are indicated along with the $Ab_{65}Cc_{35}$ composition of Lee & Wyllie (1996). The grey arrow from the BK66 starting composition to the liquid represents the effect of crystallizing 21% calcite as estimated by mass balance.

variations with respect to the solid phases that are in equilibrium with one or two liquids. The Ab–Cc join does not cut the 0·2 and 0·5 GPa two-liquid solvus (Fig. 6a and b). However, the Ne–Cc joins cuts the 0·5 GPa two-liquid field (Fig. 6a) and grazes the edge of the 0·2 GPa solvus (Fig. 6b). Further contraction of the two-liquid field at 0·1 GPa (Fig. 6a) precludes immiscibility for compositions on the Ne–Cc join, in contrast to the suggestion of Lee & Wyllie (1994). The 1·5 GPa and 1275°C $Ab_{65}Cc_{35}$ data point of Lee & Wyllie (1996) and the RB63 run are consistent; both contain a single liquid, with bulk compositions that lie outside the solvus (Fig. 6c).

The low-Na_2O experiments at 1·5 GPa proved particularly difficult to interpret. In addition to the 'globular' calcite, several silicate solid phases are present in experiments at temperatures below 1275°C. Calcite and plagioclase are common phases for lower bulk Al_2O_3/SiO_2 ratios, being replaced by calcite and scapolite (±plagioclase and nepheline) at higher Al_2O_3/SiO_2. Scapolite shows a range of compositions (from 0 to 4 wt % Na_2O) along a join from meionite towards albite. At lower pressures (0·2 and 0·5 GPa), wollastonite and melilite co-crystallize with calcite. The overall effect of these solid phases precipitating is to increase the bulk Na_2O content of the equilibrium liquid(s), effectively limiting experimental access to the low-alkali part of the two-liquid field (e.g. see Fig. 6c). This solid phase effect complicated one of our objectives, which was to establish the low Na_2O limit of the two-liquid solvus. As a result, additional experiments were performed at higher temperatures to eliminate the solid phase(s).

The effect of temperature on the two-liquid solvus at 1·5 GPa is illustrated in Fig. 7a. The 1275°C data from Fig. 6c are compared with a number of runs at 1325°C, and a series of variable temperature experiments using a single (RB100) bulk composition (listed in Table 3). Also shown in Fig. 7a are the bulk compositions of four 1·5 GPa, 1300°C experiments by Lee & Wyllie (1996) that lie along the Ab–Cc join. Their inferred position for a

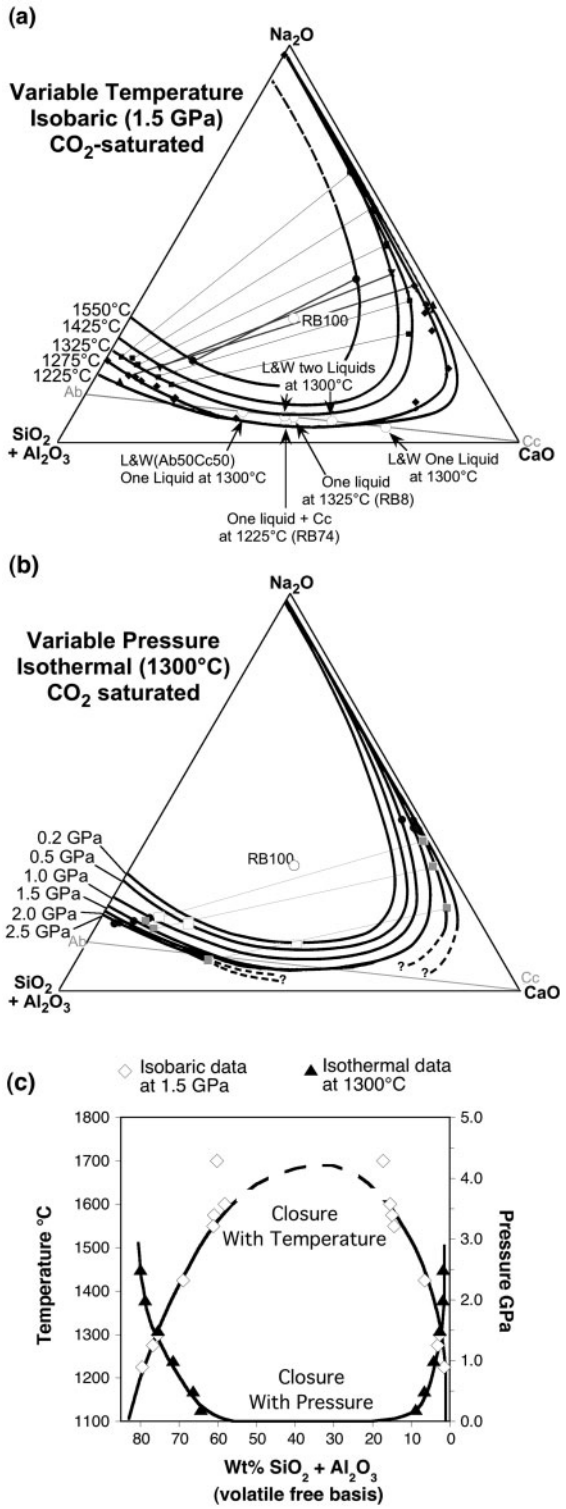

Fig. 7. The effect of varying temperature and total pressure (with $P_{CO2} = P_{tot}$) on the two-liquid solvus. (a) The closure of the two-liquid field with increasing temperature. The positions of bulk compositions and phase relations of Lee & Wyllie (1996) at 1300°C along the albite–calcite join are also indicated. Tie-lines are shown for the 1325°C data. Selected starting compositions are shown as open circles, liquid compositions at 1225°C as filled triangles, 1275°C as filled diamonds, 1325°C as filled squares, 1425°C as inverted filled triangles and 1550°C as filled circles. (b) The position of the two-liquid solvus as a function of pressure is estimated using 1300°C experiments for bulk composition RBl00 (circles) and estimated solvus positions from Fig. 6a–c (adjusted from 1250 to 1275°C). Also shown in grey are the starting compositions (open squares) and analysed 1·0 GPa, 1300°C liquid compositions (filled squares) from Lee & Wyllie (1997a). (c) *T*–*X* and *P*–*X* representations of the two-liquid solvus. The experimental data for the RBl00 bulk composition illustrate solvus closure with increasing temperature (*T*–*X*), or decreasing pressure (*P*–*X*). The data at 0·5, 0·2 and 0·1 GPa are for 1250°C. The bulk composition for the 0·5 GPa experiment (BK42) is not the same as for RBl00, but the tie-line for the conjugate liquids passes through that point. The high-temperature closure of the field (dashed line) is discussed in the text.

portion of the one-liquid–two-liquid phase boundary at 1300°C is consistent with the data of this study (but see further discussion above).

The effect of increasing pressure from 0·1 to 2·5 GPa for isothermal, CO_2-saturated conditions is illustrated in Fig. 7b. Experiments at 2·0 and 2·5 GPa were confined to moderate to high alkali contents as the low-alkali experiments were plagued by precipitation of solid phases. We have no evidence to show whether the two-liquid field is closed off at low alkali content in a similar way to the 1·5 GPa solvus. As a result we have drawn a dashed line to estimate the general topology of these solvi. The two-liquid field expands with increasing pressure, consistent with previous studies (e.g. Freestone & Hamilton, 1980). The significant expansion of the two-liquid field between 0·1 and 1·5 GPa should be noted, in contrast to a much more limited expansion between 1·5 and 2·5 GPa. Lee & Wyllie (1996) suggested a significant expansion of the two-liquid field from 1·0 to 2·5 GPa, but their experiments were limited to low alkali compositions along the Ab–Cc join. Also shown in Fig. 7b are the 1300°C, 1·0 GPa data from Lee & Wyllie (1997). These experiments have a very high Al_2O_3/SiO_2 wt % ratio of 0·76 (unrealistic for natural magmas), and although the silicate liquid compositions are broadly consistent with our data, the carbonate liquids plot well outside our 1·0 GPa solvus (i.e. at lower $SiO_2 + Al_2O_3$ concentrations). This may be an analytical artefact of the Lee & Wyllie (1997*a*) dataset, as noted above [i.e. see the variable and extended range of carbonate liquid compositions presented in fig. 5 of Lee & Wyllie (1997*a*)]. Alternately, this could be related to the extremely high Al_2O_3/SiO_2 ratios of these bulk compositions.

Figure 7c illustrates both the isobaric and isothermal closure of the solvus with increasing temperature or decreasing pressure for the RBl00 bulk starting composition (Table 3). The temperature effect is clearly illustrated from 1225 to 1550°C. However, from 1550 to 1700°C the liquids appears to unmix during the quench, so it is not possible to construct a smooth curve to the consolute point. The textures produced in the highest temperature runs

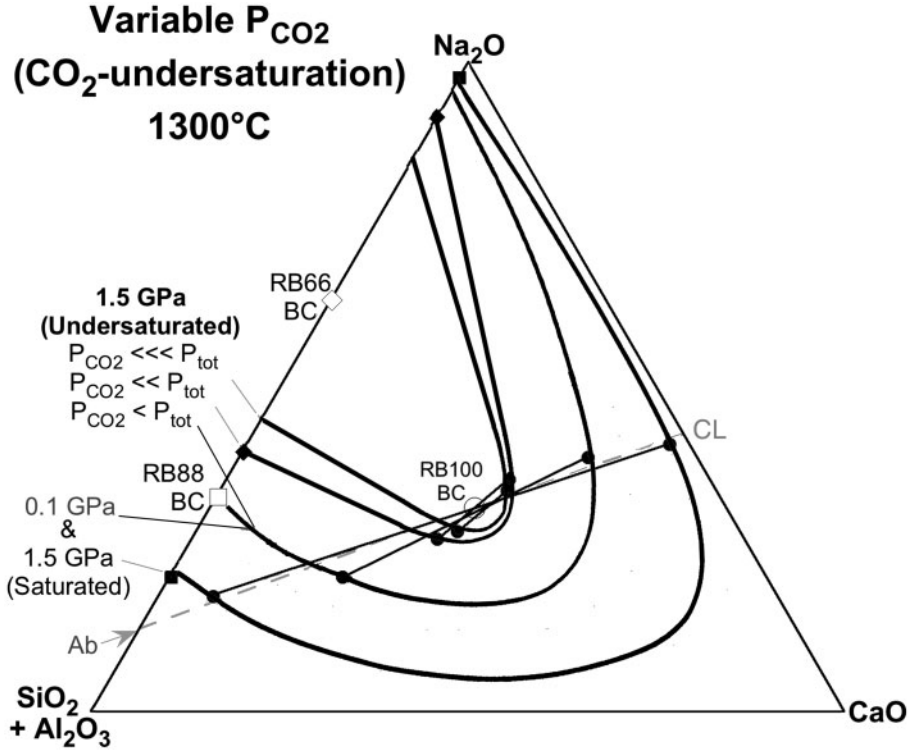

Fig. 8. The effect of P_{CO2} on solvus closure. The original CO_2 content of the RBl00 bulk composition is 31·79 wt %, but this was reduced to 24·79, 22·03 and 19·80 wt % in the CO_2-undersaturated experiments. Compositions for CO_2-saturated (RB88, squares) and CO_2-undersaturated (RB66, diamonds) experiments are also included to show the effect of P_{CO2} on solvus closure along the CaO-free join. The 0·1 GPa, 1300°C CO_2-saturated solvus is estimated from Fig. 5a. The dashed grey line is the trace of the projection plane used in Fig. 9a.

are similar to the intermingling liquids illustrated in Fig. 1b, but are more heterogeneous and very difficult to analyze. The average of several analyses suggests a comparable solvus width at both 1700°C and 1550°C. As a result, 1550°C may represent a 'closure' temperature for the piston cylinder quench rate.

The effect of CO_2 undersaturation

Any melt or magma is considered to be CO_2-undersaturated (i.e. $P_{CO2} < P_{total}$) if the CO_2 content is lower than that required to saturate one (or both) liquids and no excess fluid phase is present, or if other volatile phases such as water or halogens are also present to dilute the CO_2-bearing fluid. In experiments with graphite present, it is also possible that CO (or even CH_4 with water present) might be produced to dilute the CO_2. In nature, it is unlikely that silicate magmas generated in the mantle will be CO_2-saturated (i.e. totally free of other volatiles such as water). It is therefore important to understand the effect of CO_2 partial pressure on the solvus.

In this study, the effect of CO_2 undersaturation ($P_{CO2} < P_{total}$) was determined at a P_{total} of 1·5 GPa, by varying the loaded bulk CO_2 content for a fixed starting composition (RBl00) and fixed temperature (1300°C). This was achieved by devolatilizing an aliquot of the RBl00 starting mix and adding this back to the original mix in varying proportions. The resultant bulk composition, CO_2 content, and the quenched liquid compositions are listed in Table 3, with the data plotted in Figs 8 and 9a. RBl00 samples loaded with 31·8 wt % CO_2 showed clear evidence of excess fluid during the run (i.e. $P_{CO2} = P_{total}$). The 1·5 GPa experiments with lower bulk CO_2 contents show no evidence of excess fluid and there is a concomitant reduction in the width of the two-liquid field (Fig. 8). Reducing by 25% the bulk CO_2 from 31·8 to 24·8 wt % at 1·5 GPa produces a conjugation line similar in width to the 0·1 GPa CO_2-saturated solvus (Fig. 8). The runs with 22·03 and 19·08 wt % CO_2 produced even narrower two-liquid fields, with intermingling silicate and carbonate liquid textures (see Fig. 1b). Previously, Koster van Groos & Wyllie (1968) noted a reduction in the size of the two-liquid field for experiments in Ab–sodium carbonate (Nc) with 20 wt % H_2O, this effect being very significant for experiments with 50% H_2O, as compared with the equivalent H_2O-free runs. The addition of H_2O in these experiments has reduced $P_{CO2} < P_{total}$ and thus reduced the width of the two-liquid field. Similar results with respect to the reduction of the width of the two-liquid

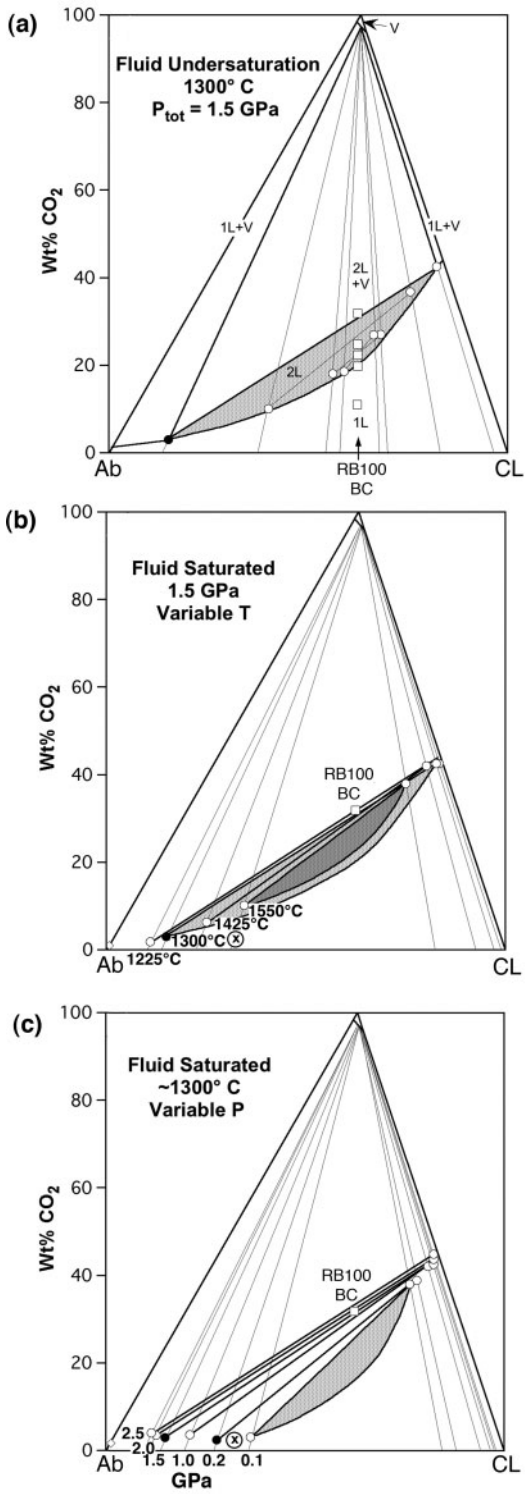

Fig. 9. The two-liquid solvus in CO_2 space for changes in (a) CO_2 undersaturation, (b) temperature and (c) pressure. These figures represent the plane from CO_2, to a line passing through Ab (albite) and the RBl00 bulk composition to the CaO–Na_2O side of the ternary diagram (grey dashed line in Fig. 8), with some compositions projected a short distance onto this plane. Experiments using the RBl00 starting composition (or near equivalents) from Figs 7a, b and 8 are used to illustrate the approximate CO_2 content of immiscible liquids. Open squares are bulk starting compositions, filled circles represent LECO data points; open circles are estimated CO_2 content using the EMP totals shortfall. In (a) the geometry of the isothermal, isobaric two-liquid field is shown using the undersaturated, variable bulk CO_2 experiments from Fig. 8. Field boundaries are denoted by black line. In (b) and (c) the change in position of the two-liquid fields as a function of temperature (b) and pressure (c) is illustrated using the fluid-saturated 'end points' from Fig. 7. The CO_2 solubilities at Ab are albite data from Brooker *et al.* (1999). The approximate limits of selected two-liquid fields (grey shading) are partly schematic. The composition denoted by X in a circle is discussed in the text. Grey projection lines onto the baseline are given as a visual guide.

solvus with CO_2 undersaturation have been described in detail by Brooker (1998) for a nephelinite–carbonate bulk composition.

Experiment RB66 is a further example of a CO_2-undersaturated starting composition and is compared with the CO_2-saturated equivalent run RB88 in Fig. 8. In this case, CO_2 undersaturation in the RB66 experiment arises from introducing a significant amount of Na_2O into the starting composition as a silicate component, rather than as Na_2CO_3 (see Table 2). This highlights an important consideration in experimental design, especially at higher pressures where the silicate liquid has an increased CO_2 demand (i.e. high solubility) in addition to the 'stoichiometric' requirements of the carbonate liquid. An insufficient content of loaded CO_2 and/or production of CO (in equilibrium with graphite capsule liners) has clearly produced CO_2-undersaturated conditions and a concomitant reduction of the two-liquid fields in the experiments of Baker & Wyllie (1990) and Lee & Wyllie (1997*b*). These results may well simulate some specific situations that occur in nature, but they do not represent the maximum possible width of the two-liquid field at the stated pressure and temperatures. As such, they cannot be compared with experiments that have $P_{CO2} = P_{total}$. The Lee & Wyllie (1997*b*) claim that increased MgO is solely responsible for the extreme solvus contraction is unlikely to be true. However, we note that we have observed a limited contraction of the solvus at CO_2-saturated conditions when 14 wt % MgO is added to the SNAC + CO_2 system (unpublished data), and that Freestone & Hamilton (1980) also observed a reduction in the width of the two-liquid field with the addition of 7 wt % MgO.

The solvus in CO_2 space

The CO_2 data, as determined by LECO for silicate liquids, and by microprobe totals shortfall for silicate and carbonate liquids, have been used to construct phase diagrams for the plane from CO_2 to a tie-line from albite through the RBl00 bulk composition to the Na_2O–CaO sideline (Fig. 8). An isobaric, isothermal representation of the phase relations illustrates the closure of the two-liquid field as a function of decreasing CO_2 content (Fig. 9a).

The two-liquid field becomes slightly narrower with increasing temperature (Fig. 9b). However, the one-liquid to two-liquid phase boundaries follow a similar path to those in Fig. 9a with respect to CO_2 space, with the CO_2 content decreasing as the two-liquid field expands to more aluminosilicate-rich compositions. Similar phase relations were shown for a more complex composition by Brooker (1998).

This contrasts strongly with the one-liquid to two-liquid phase boundaries shown in Fig. 9c, where the CO_2 content of the silicate liquids remains relatively constant because of the compositional dependence of CO_2 solubility and the change in composition of the silicate liquid with pressure (this may represent a 'feedback' mechanism that is an important part of the immiscibility process). This illustrates the important principle that for an ascending, undersaturated, low-CO_2 silicate magma (corresponding to the point marked by X in circle in Fig. 9b and c), intersection with a two-liquid field and exsolution of a carbonate liquid is more likely to occur as a result of decreasing pressure on approaching the Earth's surface, rather than a decrease in temperature. This is somewhat counter-intuitive, given that the CO_2-saturated two-liquid field decreases in size with decreasing pressure; that is, the two-liquid field on a CO_2 projected plot tends to contract away from normal magmatic compositions as the magma rises (see also discussion by Brooker, 1998).

The spinodal curve inside the two-liquid solvus

In this study, the preferred method of determining the extent of the two-liquid field was to utilize a bulk composition well inside the estimated two-liquid field, so that large volumes of each liquid are produced and available for analysis. However, a secondary constraint can be added by utilizing a number of bulk compositions that approach the two-liquid solvus from the one-liquid field, thus confirming the one-liquid to two-liquid phase boundary. This also simulates the most likely situation in nature, where crystal fractionation might increase the alkali and CO_2 content of a silicate liquid, forcing it towards the two-liquid solvus (e.g. Kjarsgaard & Hamilton, 1989*a*; Kjarsgaard *et al.*, 1995; Kjarsgaard, 1998). In theory, the use of variable starting compositions and visual identification of the resultant phase assemblage (i.e. one liquid or two liquids), should have the advantage of avoiding errors associated with analysis of the quenched liquids. Both the 'liquid composition analysis' as well as the 'variable bulk composition' techniques have been used in this study, as was also done, in part, by Lee & Wyllie (1996, 1997*a*).

In our study, we found that the position of the solvus was not reproduced by the two experimental methods (not even within analytical or experimental error). Experiments on bulk compositions just inside the two-liquid solvus typically remained as a single liquid. This is most pronounced for bulk compositions inside the silicate limb of the solvus, and is more difficult to detect for bulk compositions just inside the carbonate limb of the solvus. Examples of this effect are illustrated by 0·2 GPa run BK32 (Fig. 6a), and 0·5 GPa run BK117 (Fig. 6b) where the bulk compositions are clearly inside the two-liquid solvus, but only one silicate liquid is produced. Importantly, the CO_2 content of these silicate glasses (see Table 2) is much greater than expected. Non-equilibrium single liquids with supersaturated CO_2 contents are almost certainly due to a free energy effect, as illustrated in Fig. 10. This free-energy effect inhibits immiscible separation for compositions between the two-liquid solvus and the spinodal curve and leads to supersaturation in CO_2, instead of exsolution of a carbonate liquid. Although the 1·5 GPa phase relations of Lee & Wyllie (1996) for the Ab–Cc join are in good agreement with our data, the absence of analyses of conjugate liquid pair compositions limits the resolution of their one-liquid–two-liquid phase boundary to the spacing of the bulk compositions. However, it also appears possible that one ($Ab_{50}Cc_{50}$ at 1300°C) or two ($Ab_{65}Cc_{35}$ at 1275°C) of the Lee & Wyllie (1996) bulk compositions may be in the area between the solvus and the spinodal curve (see Figs 7a and 6c), resulting in inhibited unmixing and thus slightly underestimating the true width of the two-liquid field.

DISCUSSION

Petrological applications of liquid immiscibility to carbonatite genesis

Data presented in this study for the SNAC + CO_2 system suggest that the minimum alkali requirement for liquid immiscibility is *c.* 5 wt % at 1·5 GPa (Lee & Wyllie 1996, 1997*a*; this study, Figs 6 and 7). This is particularly apparent in Fig. 7a, where the two-liquid field appears to flatten out as the temperature is lowered, being 'pinned' above this minimum 5 wt % amount and expanding towards the CaO corner. It should be noted that this effect is apparent before solid phases start to precipitate. Slightly lower alkali concentrations can be realized for natural compositions, as a result of lower temperatures; for example, 4·25 wt % alkalis at 0·5 GPa and 1025°C (Kjarsgaard, 1998). Above 1·5 GPa it is unclear from our data if the solvus continues to expand towards the alkali-free baseline, but low and very low alkali (<1 wt % alkalis) concentrations have been reported for immiscible carbonate–silicate liquids in higher pressure (3·0–5·0 GPa) experiments (e.g. Dasgupta *et al.*, 2006; Thomsen & Schmidt, 2008) and for the alkali-free CMAS + CO_2 experiments of Novella & Kershav (2010) at 2·0–2·6 GPa. A highly important observation from these recent experimental studies is that alkali-free immiscible carbonates cannot be pure $CaCO_3$

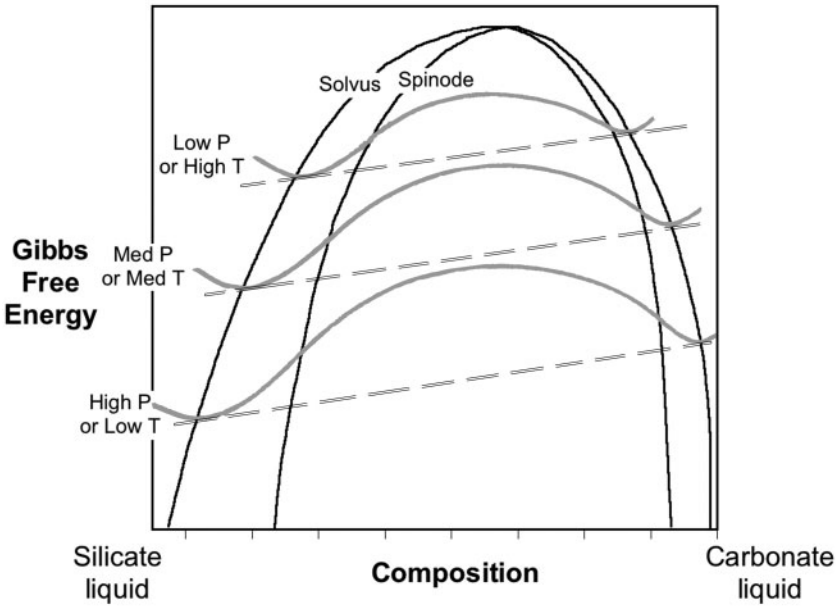

Fig. 10. Schematic representation of the theoretical Gibbs free energy surfaces (grey curves) appropriate to an immiscible solvus, as a function of composition and changing P–T conditions. The common tangents (dashed straight lines) to these surfaces illustrate that the lowest energy condition is satisfied by unmixing to give the two liquids that define the immiscible solvus (black curve). The black curve inside the solvus is the spinodal curve, which follows the inflection in the free energy surface where the curvature changes from positive to negative. Inside this dashed line, unmixing is spontaneous, but between the spinodal curve and the solvus is a region where unmixing is kinetically inhibited, requiring large compositional fluctuations (nucleation) to initiate unmixing [e.g. see Schmalzried (1981) for a detailed description].

under any conditions, as the solvus curves away from the CaO corner in the quasi-ternary diagrams.

In terms of immiscible carbonatite compositions, our study confirms the conclusions of previous studies—that low-aluminosilicate, high-alkali natrocarbonatite compositions such as those of Oldoinyo Lengai can be produced by immiscible separation from a peralkaline silicate parent (Koster van Groos & Wyllie, 1966, 1968; Freestone & Hamilton, 1980; Kjarsgaard & Peterson, 1991; Kjarsgaard *et al.*, 1995; Mitchell, 2009). At least 15 wt % alkalis in an exsolved carbonate liquid appears to be the minimum required if the aluminosilicate content is to be below 3 wt %. Low-alkali carbonatite melts can be generated by liquid immiscibility, but these exsolved carbonate liquids with less than 5 wt % alkalis must also have a significant aluminosilicate ($>\sim$10 wt % $SiO_2 + Al_2O_3$) content (Hamilton & Kjarsgaard, 1993; Lee & Wyllie 1996, 1997*a*; Kjarsgaard, 1998; Dasgupta *et al.*, 2006; Novella & Kershav, 2010; this study).

Whole-rock carbonatite analyses in the literature are dominated by examples that have $\leq$5 wt % $SiO_2 + Al_2O_3$ (Woolley & Kempe, 1989), consistent with the observation that minor quantities of ferromagnesian silicate minerals (e.g. olivine, clinopyroxene, melanite garnet, mica and amphibole) are observed in many carbonatites (Twyman & Gittins, 1987; Gittins, 1989; Hogarth, 1989). In contrast, numerous carbonatites exhibit no or very limited contents of these mineral phases and thus have very low silica and alkali contents. For low-alkali carbonatites, this could be taken to exclude an immiscible origin in favour of a direct mantle carbonatite melt (e.g. Dalton & Wood, 1993). For some cases this may be true, but an equally viable option is that minor crystal fractionation of silicate minerals from a separated, parental immiscible carbonate melt would easily deplete both aluminosilicate and alkali components (e.g. Macdonald *et al.*, 1993; Kjarsgaard *et al.*, 1995; Kjarsgaard, 1998; Petibon *et al.*, 1998), and the release of alkali-rich (fenitizing) fluids (Le Bas, 1987) would further deplete alkalis. Fractionation processes would be enhanced by the high density contrast and the low viscosity of the carbonatite melt. More detailed experimental (and field) work is required to find methods for differentiating between carbonatites produced by these two processes.

Experimental data for low-alkali nephelinite (Kjarsgaard, 1998), melilitite (Kjarsgaard & Hamilton, 1989*b*) and multicomponent synthetic systems (Suk, 2001, 2003) support the general features observed for the alkali-poor closure of the two-liquid field in the $SNAC + CO_2$ system. In this context, the results from our simple system experiments are highly relevant to understanding parental carbonatite magma compositions and petrogenetic models. We speculate further on this subject in Fig. 11, where low-pressure (0·2 GPa) and high-pressure

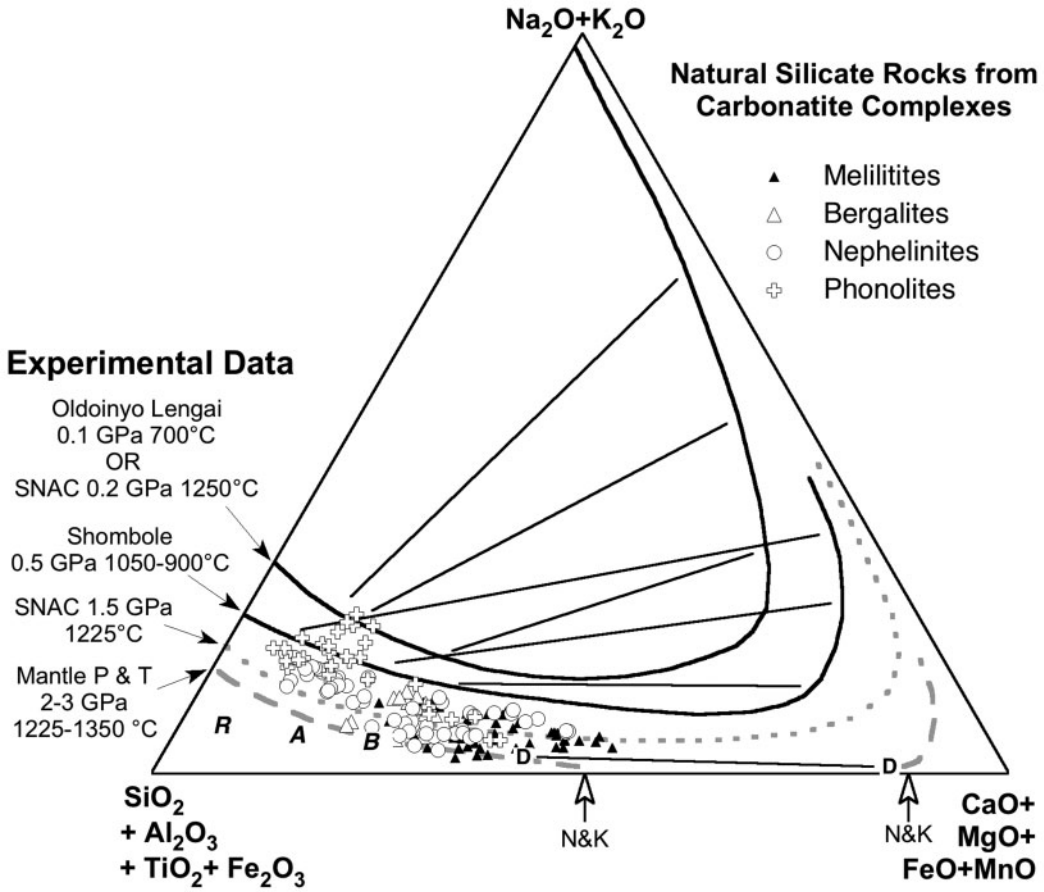

Fig. 11. The compositions of alkali silicate volcanic and hypabyssal rocks found in carbonatite complexes, compared with experimental CO_2-saturated two-liquid solvi in SNAC (this study). The data for more complex compositions are plotted by adding the extra components to each apex as shown (after Freestone & Hamilton, 1980). The SNAC solvus positions at 1·5 GPa, 1225°C and 0·2 GPa, 1250°C are from this study. Also shown is the 0·5 GPa solvus for a nephelinite composition compiled for a range of temperatures (1050–900°C) from Kjarsgaard & Peterson (1991). The 0·2 GPa 1250°C SNAC solvus passes through data for experiments on Oldoinyo Lengai phonolites at 0·1 GPa and 700°C (Kjarsgaard *et al.* 1995). The tie-lines for these data are shown as representative lines for the Shombole experiments. The 'mantle' solvus for 2·0–3·0 GPa is estimated from this study and the compositions of Dasgupta *et al.* (2006) and Novella & Keshav (2010) labelled D and N&K, respectively. The compositions of generic basalt (*B*), andesite (*A*) and rhyolite (*R*) are also shown.

(1·5 GPa) SNAC solvi are plotted along with less well-constrained solvi determined from natural compositions. The 0·2 GPa 1250°C SNAC solvus coincides with data for experiments on Oldoinyo Lengai compositions at lower pressure and temperature (0·1 GPa and 700°C; Kjarsgaard *et al.*, 1995). This highlights the fact that any solvus drawn on this diagram can represent a range of CO_2 pressure (or even partial pressure) and temperature combinations, the contraction related to decreasing pressure counteracted by decreasing temperature in ascending magmas. Also shown is the 0·5 GPa solvus for experiments on natural nephelinites from Shombole (Kjarsgaard, 1998). This solvus is polythermal, representing temperatures from 1050 to 900°C (hence the slightly 'distorted' shape). This solvus plots inside the position of the SNAC 0·5 GPa, 1250°C solvus (see Fig. 6b), consistent with the lower temperatures involved. Also plotted in Fig. 11 is an estimated high-pressure solvus (2·0–3·0 GPa) based on the 2·5 GPa, 1300°C SNAC data of this study, the CMAS data of Novella & Kershav (2010) at 2·0–2·6 GPa (to temperatures above 1500°C), and the more complex natural compositions of Dasgupta *et al.* (2006) at 3·0 GPa and 1225–1350°C. It should be noted that we have not utilized the MgO-bearing 2·5 GPa 1250°C solvus from Brooker (1998). This would plot inside the SNAC 1·5 GPa, 1250°C solvus in a position close to the Shombole 0·5 GPa data. The additional MgO in the Brooker (1998) experiments might explain some of the discrepancy between the SNAC and natural composition data, but not the difference from the Dasgupta *et al.* (2006) results. This may represent a problem with comparing data from simple and complex compositions on the quasi-ternary plot. However, one

other possibility is that either CO (produced by reduction of CO_2 by FeO), or H_2O was present in the Brooker (1998) experiments, producing a CO_2 partial pressure slightly below 2·5 GPa. Significant fluorine in the lower alkali compositions may also have diluted the CO_2.

Although there may be problems with representing more complex compositions and solvi topology on the simple quasi-ternary plot, we have plotted the compositions of a number of alkali silicate volcanic and hypabyssal rocks from carbonatite complexes worldwide. Taken at face value (e.g. CO_2-saturated conditions), Fig. 11 would suggest that melilitites would exsolve a carbonatite melt only at mantle conditions and this would be low in alkalis or alkali free with a significant $SiO_2 + Al_2O_3$ component. Bergalites would need shallow mantle to deep crustal conditions and the exsolved carbonatite is more likely to have a small alkali component. This may be significant as calcio-carbonatite lapilli tuffs associated with the Kaiserstuhl bergalites have exceptionally high $CaCO_3$ compositions and are inferred to be molten at atmospheric pressure (Keller, 1989), where dissociation to CaO and CO_2 should occur. A small amount of alkalis (now lost) has been suggested as one solution to this dissociation problem (Jago & Gittins, 1991), and the solvi at 10% alkalis would also allow the observed low $SiO_2 + Al_2O_3$ contents. Primitive nephelinites may be produced at higher mantle temperatures than melilitites (owing to higher degrees of melting; Wallace & Green, 1988) or be the lower temperature products of fractionation. As a result they cover the widest range of conditions from mantle to crust and may exsolve carbonatites with alkali contents ranging from very low up to about 50 wt %. Fractionated, lower-temperature phonolites appear most suited to exsolving an alkali-rich carbonate liquid at mid- to shallow crustal conditions. The alkali content is increased further by the rotation of the tie-lines for these highly peralkaline compositions (Fig. 11; Kjarsgaard & Peterson, 1991). Also shown in Fig. 11 are the more common igneous compositions: basalt, andesite and rhyolite. It is clear that these compositions are highly unlikely to intersect immiscible conditions in the unlikely event that they become CO_2-saturated.

As illustrated previously by Brooker (1998) and confirmed in this study, the CO_2 saturation of the silicate liquid (P_{CO2} rather than P_{total}) is a highly important factor in generating an immiscible carbonate melt. In nature, the CO_2-saturated scenarios described above are unlikely to be commonplace. The amount of CO_2 in a magma generated in the mantle is a function of the CO_2 content of the source and the degree of melting. At very low degrees of partial melting, the melt produced can be carbonatitic. There are questions as to whether these small-volume melts can be extracted from the mantle, or get past the 'solidus ledge' as they ascend (e.g. Wallace & Green, 1988). At higher degrees of melting, the magmas rapidly become more silicic (e.g. Wallace & Green, 1988; Moore & Wood, 1998) and the CO_2 is probably diluted below saturation as the CO_2 source is exhausted. Natural primitive nephelinite and melilitite magmas probably contain ~4 and 8 wt % CO_2, respectively (Eggler, 1989), whereas CO_2 solubilty in melts of these compositions may be 5–10 and 10–20 wt % CO_2, respectively (Brooker *et al.*, 2001) at mantle conditions. Hence we suggest that natural magmas at pressures equivalent to mantle or lower crustal depths will be CO_2 undersaturated with respect to the two-liquid solvus. As a result, immiscibility is most likely to occur at the low CO_2-saturation demand conditions found in lower-pressure (<1·0 GPa) crustal magma chambers, or in mantle magma chambers in areas where the lithosphere has been thinned (e.g. the East African Rift or the Rhine Graben). In these lower pressure conditions, immiscibility will be induced by cooling and crystal fractionation of ferromagnesian silicate and oxide minerals that increase the alkali and CO_2 content of the residual silicate melt, which then intersects the two-liquid field that is expanding at the lower T conditions (Kjarsgaard & Hamilton, 1988, 1989*a*; Kjarsgaard *et al.*, 1995; Lee & Wyllie, 1998).

However, the contraction of the two-liquid field with decreasing pressure, as the magma approaches the surface (reduced P_{total}), possibly exaggerated by escape of CO_2 ($P_{CO2} \ll P_{total}$), may cause the readsorption of any carbonate liquid that has been exsolved and not physically separated from the parental magma. This will ensure that the preservation of actual immiscible textures in nature is very rare, but they do exist (e.g. Kjarsgaard & Peterson, 1991; Dawson *et al.*, 1992, 1994; Macdonald *et al.*, 1993). This demonstrates the importance of considering CO_2 solubility in natural two-liquid magmatic systems, and in particular the difference between CO_2-saturated and -undersaturated systems. One other composition worth considering is kimberlite; this would plot right in the middle of the two-liquid field in Fig. 11, almost on the alkali-free baseline at mantle conditions. However, the high CO_2 content common in these compositions is always 'diluted' by some significant H_2O component (Kjarsgaard *et al.*, 2009), so lower 'partial' pressure solvi would be relevant. As a result, these relatively low alkali compositions are unlikely to experience immiscible exsolution at 3·0 GPa or during ascent through the crust.

Round calcite crystals in mantle xenoliths

The presence of $CaCO_3$ 'globules' in experiments is reinterpreted in this study to reflect a solid phase (see also Macdonald *et al.* 1993; Lee & Wyllie, 1994, 1996, 1997*a*; Lee *et al.*, 1994; Brooker, 1995). This observation has direct application to the numerous reports of carbonate phases in mantle xenoliths that are either 'globules' or have immiscible-like boundaries with silicate, or occasionally

sulphide melts (e.g. Amundsen, 1987; Ionov *et al.*, 1993; Pyle & Haggerty, 1994; Schiano *et al.*, 1994; Kogarko *et al.*, 1995, 2001; Seifert & Thomas, 1995; Norman, 1998; Chalot-Prat & Arnold, 1999; Laurora *et al.*, 2001; Hurai *et al.*, 2007). Although many of these have been interpreted as quenched immiscible carbonate liquids, none of the published analyses appear to have sufficient alkalis, silica or alumina for this to be the case. Our interpretation of these globular calcite textures supports the conclusions of Ionov (1998) and Ionov & Harmer (2002), that these are rounded crystalline calcite that has precipitated from a silicate melt. The observed textures in xenoliths suggest that these calcite crystals may play an important role in reducing permeability and in trapping the residual silicate melt. When the possibilities of mosaic textures caused by inversion of high P–T calcite polymorphs, or radiating domains related to single 'christmas tree' crystals are considered, it is clear that interpretation of primary carbonate textures in mantle xenoliths can be highly complex and problematic.

CONCLUSIONS

Silicate–carbonate liquid immiscibility is clearly possible at crustal pressures, given enough alkalis (5 wt %) and a high enough CO_2 partial pressure. However, the high CO_2 demand at high (>1·0 GPa) pressures suggests that the process of liquid immiscibility is unlikely to be a common process in the mantle. Common silicate magma compositions such as tholeiitic basalt (2–3 wt % alkalis and low CO_2) cannot be parental to immiscible carbonatite melts. However, silica-undersaturated alkaline magmas (e.g. olivine nephelinite, olivine melilitite) that are produced by partial melting of a carbonated mantle source (e.g. Wallace & Green, 1988; Foley *et al.*, 2009) are certainly viable candidates to exsolve a carbonate liquid, especially as they differentiate to more evolved compositions. The carbonatite melt produced from evolved nephelinites or phonolites would be high in alkalis. This is consistent with the world's only active carbonatite volcano (Oldoinyo Lengai), but at odds with the vast majority of natural occurrences. Nephelinite or melilitite magmas appear to be the best candidates to exsolve an immiscible, low-alkali carbonatite melt that will also have a significant component of $SiO_2 + Al_2O_3$. More work is required to link these compositions to observed rock compositions.

ACKNOWLEDGEMENTS

Both authors had the great pleasure of numerous stimulating discussions and written correspondence with Pete Wyllie during the 1990s on the silicate–carbonate liquid immiscibility and round calcite problems. We thank Dave Hamilton for help and advice, John Holloway for access to facilities at ASU, and Dave Plant, Jim Clark and John Stirling for help with electron micrope at MU, ASU and GSC, respectively. Reviews from K. Bell, K. Moore, I. Veksler and L. Kogarko greatly improved this paper.

FUNDING

Financial support for this project was supplied by NERC (Grants GT4/87/GS/76 to R.A.B. and GR3/6477 to the experimental petrology laboratory at Manchester) and a Manchester University Scholarship to B.A.K. Additional support to B.A.K. for continuing carbonatite studies has been furnished by the Geological Survey of Canada. This is Geological Survey of Canada contribution # 2010-483.

REFERENCES

Amundsen, H. E. F. (1987). Evidence for liquid immiscibility in the upper mantle. *Nature* **327**, 692–695.

Baker, M. B. & Wyllie, P. J. (1990). Liquid immiscibility in a nephelinite–carbonate system at 25 kb and implications for carbonatite origin. *Nature* **346**, 168–170.

Barker, D. S. & Nixon, P. H. (1989). High-Ca, low-alkali carbonatite volanism at Fort Portal, Uganda. *Contributions to Mineralogy and Petrology* **103**, 166–177.

Bell, K., Kjarsgaard, B. A. & Simonetti, A. (1998). Carbonatites—Into the twenty-first century. *Journal of Petrology* **39**, 1839–1845.

Brey, G. P., Bulatov, V. K. & Girnis, A. V. (2009). The influence of water and fluorine on the melting of carbonated peridotite at 6 and 10 GPa. *Lithos* **112S**, 249–259.

Brooker, R. A. (1995). Carbonatite genesis; the role of liquid immiscibility to 25 kb, PhD thesis, University of Manchester.

Brooker, R. A. (1998). The effect of CO_2 saturation on silicate–carbonate immiscible systems. *Journal of Petrology* **39**, 1905–1915.

Brooker, R. A. & Hamilton, D. L. (1990). Three liquid immiscibility and the origin of carbonatites. *Nature* **346**, 459–462.

Brooker, R. A., Holloway, J. R. & Hervig, R. L. (1998). Reduction in piston cylinder experiments: The detection of carbon infiltration into platinum capsules. *American Mineralogist* **83**, 985–994.

Brooker, R. A., Kohn, S. C., Holloway, J. R., McMillan, P. F. & Carroll, M. R. (1999). CO_2 solubility, speciation and dissolution mechanisms for melt compositions along the $NaAlO_2$–SiO_2 join. *Geochimica et Cosmochimica Acta* **63**, 3549–3565.

Brooker, R. A., Kohn, S. C., Holloway, J. R. & McMillan, P. F. (2001). Structural controls on the solubility of CO2 in silicate melts. Part I: Bulk solubility data. *Chemical Geology* **174**, 225–240.

Carlson, W. D. (1983). The polymorphs of $CaCO_3$ and the aragonite–calcite transformation. In: Reeder, R. J. (ed.) *Carbonates: Mineralogy and Chemistry. Mineralogical Society of America, Reviews in Mineralogy* **11**, 191–225.

Chalot-Prat, F. & Arnold, M. (1999). Immiscibility between calciocarbonatites and silicate melts and related wall rock reactions in the upper mantle: a natural case study from Romanian mantle xenoliths. *Lithos* **46**, 627–659.

Clark, S. P. (1959). Effect of pressure on the melting points of eight alkali halides. *Journal of Chemical Physics* **31**, 1526–1531.

Dalton, J. A. & Wood, B. J. (1993). The composition of primary carbonate melts and their evolution through wallrock reaction in the mantle. *Earth and Planetary Science Letters* **119**, 511–525.

Dasgupta, R., Hirschmann, M. M. & Stalker, K. (2006). Immiscible transition from carbonate-rich to silicate-rich melts in the 3 GPa melting interval of eclogite + CO_2 and genesis of silica undersaturated ocean island lavas. *Journal of Petrology* **47**, 647–671.

Dawson, J. B. & Hawthorne, J. B. (1973). Magmatic sedimentation and carbonatitic differentiation in kimberlite sills at Benfontein, South Africa. *Journal of the Geological Society, London* **129**, 61–85.

Dawson, J. B., Smith, J. V. & Steele, I. M. (1992). 1966 ash eruption of the carbonatite volcano Oldoinyo Lengai: mineralogy of lapilli and mixing of silicate and carbonate magmas. *Mineralogical Magazine* **56**, 1–16.

Dawson, J. B., Pinkerton, H., Pyle, D. M. & Nyamweru, C. (1994). June 1993 eruption of Oldoinyo Lengai, Tanzania: Exceptionally viscous and large carbonatite lava flows and evidence for coexisting silicate and carbonate magmas. *Geology* **22**, 769–864.

Deans, T. & Roberts, B. (1984). Carbonatite tuffs and lava clasts of the Tinderet foothills, western Kenya: a study of calcified natrocarbonatite. *Journal of the Geological Society, London* **141**, 563–580.

Eggler, D. H. (1989). Carbonatites, primary mantle melts and mantle dynamics. In: Bell, K. (ed.) *Carbonatites: Genesis and Evolution*. London: Unwin Hyman, pp. 561–579.

Foley, S. F., Yaxley, G. M., Rosenthal, A., Buhre, S., Kiseeva, E. S., Rapp, R. P. & Jacob, D. E. (2009). The composition of near-solidus melts of peridotite in the presence of CO_2 and H_2O between 40 and 60 kbar. *Lithos* **112S**, 274–283.

Freestone, I. C. & Hamilton, D. L. (1980). The role of liquid immiscibility in the genesis of carbonatites: an experimental study. *Contributions to Mineralogy and Petrology* **73**, 105–117.

Gittins, J. (1989). The origin and evolution of carbonatite magmas. In: Bell, K. (ed.) *Carbonatites: Genesis and Evolution*. London: Unwin Hyman, pp. 580–600.

Guzmics, T., Mitchell, R. H., Szabo, C., Berkesi, M., Milke, R. & Abart, R. (2010). Carbonatite melt inclusions in coexisting magnetite, apatite and monticellite in Kerimas calciocarbonatite, Tanzania: melt evoluion and petrogenesis. *Contributions to Mineralogy and Petrology* (in press).

Halama, R., Vennemann, T., Siebel, W. & Markl, G. (2005). The Gronnedal–Ika carbonatite–syenite complex, South Greenland: Carbonatite formation by liquid immiscibility. *Journal of Petrology* **46**, 191–217.

Hamilton, D. L. & Kjarsgaard, B. A. (1993). The immiscibility of silicate and carbonate melts. *South African Journal of Geology* **96**, 139–142.

Hamilton, D. L., Freestone, I. C., Dawson, J. B. & Donaldson, C. H. (1979). Origin of carbonatites by liquid immiscibility. *Nature* **279**, 52–54.

Hogarth, D. D. (1989). Pyrochlore, apatite and amphibole: distinctive minerals in carbonatite. In: Bell, K. (ed.) *Carbonatites: Genesis and Evolution*. London: Unwin Hyman, pp. 105–148.

Hurai, V., Huraiova, M., Konecny, P. & Thomas, R. (2007). Mineral–melt–fluid composition of carbonate-bearing cumulate xenoliths in Tertiary alkali basalts of southern Slovakia. *Mineralogical Magazine* **71**, 63–79.

Ionov, D. A. (1998). Trace element composition of mantle-derived carbonates and coexisting phases in peridotite xenoliths from alkali basalts. *Journal of Petrology* **39**, 1931–1941.

Ionov, D. & Harmer, R. E. (2002). Trace element distribution in calcite – dolomite carbonatites from Spitskop: inferences for differentiation of carbonatite magmas and the origin of carbonates in mantle xenoliths. *Earth and Planetary Science Letters* **198**, 495–510.

Ionov, D. A., Dupuy, C., O'Reilly, S. Y., Kopylova, M. G. & Genshaft, Y. S. (1993). Carbonated peridotite xenoliths from Spitsbergen: implications for trace element signatures of mantle carbonate metasomatism. *Earth and Planetary Science Letters* **119**, 283–297.

Ionov, D. A., O'Reilly, S. Y., Genshaft, Y. S. & Kopylova, M. G. (1996). Carbonate-bearing mantle peridotite xenoliths from Spitsbergen: phase relationships, mineral compositions and trace-element residence. *Contribributions to Mineralogy and Petrology* **125**, 375–392.

Jago, B. C. & Gittins, J. (1991). Extrusive carbonatites: their origins reappraised in the light of new experimental data. *Geological Magazine* **128**, 301–305.

Keller, J. (1989). Extrusive carbonatites and their significance. In: Bell, K. (ed.) *Carbonatites: Genesis and Evolution*. London: Unwin Hyman, pp. 70–88.

Kjarsgaard, B. A. (1990). Nephelinite–carbonatite genesis: Experiments on liquid immiscibility in alkali silicate–carbonate systems, PhD thesis, University of Manchester.

Kjarsgaard, B. A. (1998). Phase relations of a carbonated high-CaO nephelinite at 0·2 and 0·5 GPa. *Journal of Petrology* **39**, 2061–2075.

Kjarsgaard, B. A. & Hamilton, D. L. (1988). Liquid immiscibility and the origin of alkali-poor carbonatites. *Mineralogical Magazine* **52**, 43–55.

Kjarsgaard, B. A. & Hamilton, D. L. (1989*a*). The genesis of carbonatites by immiscibility. In: Bell, K. (ed.) *Carbonatites: Genesis and Evolution*. London: Unwin Hyman, pp. 388–404.

Kjarsgaard, B. A. & Hamilton, D. L. (1989*b*). Carbonatite origin and diversity. *Nature* **324**, 547–548.

Kjarsgaard, B. A. & Peterson, T. D. (1991). Nephelinite–carbonatite liquid immiscibility at Shombole volcano, East Africa: Petrographic and experimental evidence. *Mineralogy and Petrology* **43**, 293–314.

Kjarsgaard, B. A., Hamilton., D. L. & Peterson, T. D. (1995). Peralkaline nephelinite/carbonatite liquid immiscibility: Comparison of phase compositions in experiments and natural lavas from Oldoinyo Lengai. In: Bell, K. & Keller, J. (eds) *Carbonatite Volcanism—Oldoinyo Lengai and the Petrogenesis of Natrocarbonatites. IAVCEI Proceedings in Volcanology* **4**, 163–190.

Kjarsgaard, B. A., Pearson, D. G., Tappe, S., Nowell, G. M. & Dowall, D. P. (2009). Geochemistry of hypabyssal kimberlites from Lac de Gras: comparisons to a global database and applications to the parent magma problem. *Lithos* **112S**, 236–248.

Kogarko, L. N., Henderson, C. M. B. & Pacheco, H. (1995). Primary Ca-rich carbonatite magma and carbonate–silicate–sulphide liquid immiscibility in the upper mantle. *Contributions to Mineralogy and Petrology* **121**, 267–274.

Kogarko, L. N., Kurat, G. & Ntaflos, T. (2001). Carbonate metasomatism of the oceanic mantle beneath Fernando de Noronha Island, Brazil. *Contributions to Mineralogy and Petrology* **140**, 577–587.

Koster van Groos, A. F. (1975). The effect of high CO_2 pressure on alkalic rocks and its bearing on the formation of alkalic ultrabasic rocks and the associated carbonatites. *American Journal of Science* **275**, 163–185.

Koster van Groos, A. F. & Wyllie, P. J. (1966). Liquid immiscibility in the system Na_2O–Al_2O_3–SiO_2–CO_2 at pressures up to 1 kilobar. *American Journal of Science* **264**, 234–255.

Koster van Groos, A. F. & Wyllie, P. J. (1968). Liquid immiscibility in the join $NaAlSi_3O_8$–Na_2CO_3–H_2O. *American Journal of Science* **266**, 932–967.

Koster van Groos, A. F. & Wyllie, P. J. (1973). Liquid immiscibility in the join $NaAlSi_3O_8$–$CaAl_2Si_2O_8$–Na_2CO_3–H_2O. *American Journal of Science* **273**, 465–487.

Kushiro, I. (1976). A new furnace assembly with a small temperature gradient in solid-media apparatus. *Carnegie Institution of Washington Yearbook* **75**, 832–833.

Laurora, A., Mazzucchelli, M., Rivalenti, G., Vannucci, R., Zanetti, A., Barbieri, M. A. & Cingolani, C. A. (2001). Metasomatism and melting in carbonated peridotite xenoliths from the mantle wedge: The Gobernador Gregores case (southern Patagonia). *Journal of Petrology* **42**, 69–87.

Le Bas, M. J. (1987). Nephelinites and carbonatites. In: Fitton, J. G. & Upton, B. G. J. (eds) *Alkaline Igneous Rocks. Geological Society, London, Special Publications* **30**, 53–85.

Lee, W.-J. & Wyllie, P. J. (1994). Experimental data bearing on liquid immiscibility, crystal fractionation, and the origin of calciocarbonatites and natrocarbonatite. *International Geological Review* **36**, 797–819.

Lee, W.-J. & Wyllie, P. J. (1996). Liquid immiscibility in the join $NaAlSi_3O_8$–$CaCO_3$ to 2·5 GPa and the origin of calciocarbonatite magmas. *Journal of Petrology* **37**, 1125–1152.

Lee, W.-J. & Wyllie, P. J. (1997*a*). Liquid immiscibility in the join $NaAlSiO_4$–$NaAlSi_3O_8$–$CaCO_3$ at 1·0 GPa: implications for crustal carbonatites. *Journal of Petrology* **38**, 1113–1135.

Lee, W.-J. & Wyllie, P. J. (1997*b*). Liquid immiscibility between nephelinite and carbonatite from 1·0 to 2·5 GPa compared with mantle melt compositions. *Contributions to Mineralogy and Petrology* **127**, 1–16.

Lee, W.-J. & Wyllie, P. J. (1998). Processes of crustal carbonatite formation by liquid immiscibility and differentiation, elucidated by model systems. *Journal of Petrology* **39**, 2005–2013.

Lee, W.-J., Wyllie, P. J. & Rossman, G. R. (1994). CO_2-rich glass, round calcite crystals and no liquid immiscibility in the system CaO–SiO_2–CO_2 at 2·5 GPa. *American Mineralogist* **79**, 1135–1144.

Maaloe, S. & Wyllie, P. J. (1975). The join grossular–calcite through the system CaO–SiO_2–Al_2O_3–CO_2 at 30 kilobars: crystallization range of silicates and carbonates on the liquidus. *Earth and Planetary Science Letters* **28**, 205–208.

Macdonald, R., Kjarsgaard, B. A., Skilling, I. P., Davies, G. R., Hamilton, D. L. & Black, S. (1993). Liquid immiscibility between trachyte and carbonate in ash flow tuffs from Kenya. *Contributions to Mineralogy and Petrology* **114**, 276–287.

Mattey, D. P., Taylor, W. R., Green, D. H. & Pillinger, C. T. (1990). Carbon isotopic fractionation between CO_2, vapour, silicate and carbonate melts: an experimental study to 31 kbar. *Contributions to Mineralogy and Petrology* **104**, 492–505.

McDade, P., Wood, B., Van Westrenen, W., Brooker, R., Gudmundsson, G., Soulard, H., Najorka, J. & Blundy, J. (2002). Pressure corrections for a selection of piston-cylinder assemblies. *Mineralogical Magazine* **66**, 1021–1028.

Mitchell, R. H. (1997). *Kimberlites, Orangeites, Lamproites, Melilitites, and Minettes: a Petrographic Atlas*. Thunder Bay, ON: Almaz Press.

Mitchell, R. H. (2009). Peralkaline nephelinite-natrocarbonatite immiscibility and carbonatite assimilation at Oldoinyo Lengai, Tanzania. *Contributions to Mineralogy and Petrology* **158**, 589–598.

Moore, K. & Wood, B. J. (1998). The transition from carbonate to silicate melts in the CaO–MgO–SiO_2–CO_2 system. *Journal of Petrology* **39**, 1943–1952.

Nielsen, T. F. D. (1980). The petrology of a melilitolite, melteigite, carbonatite and syenite dyke system in the Gardiner complex, East Greenland. *Lithos* **13**, 181–197.

Norman, M. D. (1998). Melting and metasomatism in the continental lithosphere: laser ablation ICPMS analysis of minerals in spinel lherzolites from eastern Australia. *Contributions to Mineralogy and Petrology* **130**, 240–255.

Novella, D. & Keshav, S. (2010). Silicate melt–carbonatite liquid immiscibility reconsidered in the system CaO–$MgOAl_2O_3$–SiO_2–CO_2 at 2–3 GPa. (Conference Abstract.) France: EMPG XIII, Toulouse.

Petibon, C. M., Kjarsgaard, B. A., Jenner, G. A. & Jackson, S. E. (1998). Phase relationships of a silicate-bearing natrocarbonatite from Oldoinyo Lengai at 20 and 100 MPa. *Journal of Petrology* **39**, 2137–2151.

Pyle, J. M. & Haggerty, S. E. (1994). Silicate–carbonate liquid immiscibility in upper-mantle eclogites: Implications for natrosilicic and carbonatitic conjugate melts. *Geochimica et Cosmochimica Acta* **58**, 2997–3011.

Schiano, P., Clocchiatti, R., Shimuzu, N., Weis, D. & Mattielle, N. (1994). Cogenetic silica-rich and carbonate-rich melts trapped in mantle minerals in Kerguelen ultramafic xenoliths: Implications for metasomatism in the oceanic upper mantle. *Earth and Planetary Science Letters* **123**, 167–178.

Schmalzried, H. (1981). *Solid State Reactions. Monographs in Modern Chemistry*, 2nd edn. Weinheim: Wiley-Verlag Chemie, 264 p.

Seifert, F. A., Mysen, B. O. & Virgo, D. (1979). Sodium loss from sodium metasilicate melts in CO_2 and CO atmospheres. *Carnegie Institution of Washington Yearbook* **78**, 679.

Seifert, W. & Thomas, R. (1995). Silicate–carbonate immiscibility: a melt inclusion study of olivine melilitite and wehrlite xenoliths in tephrite from the Elbe Zone, Germany. *Chemie der Erde* **55**, 263–279.

Suk, N. I. (2001). Experimental study of liquid immiscibility in silicate–carbonate systems. *Petrology* **9**, 477–487.

Suk, N. I. (2003). Experimental investigation of carbonate–silicate liquid immiscibility with applications to the formation of barium–strontium carbonatites. *Petrology* **11**, 400–405.

Thomsen, T. B. & Schmidt, M. W. (2008). Melting of carbonated pelites at 2·5–5·0 GPa, silicate–carbonate liquid immiscibility, and potassium–carbon metasomatism of the mantle. *Earth and Planetary Science Letters* **267**, 17–31.

Twyman, J. D. & Gittins, J. (1987). Alkalic carbonatite magmas: parental or derivative? In: Fitton, J. G. & Upton, B. G. J. (eds) *Alkaline Igneous Rocks Geological Society, London, Special Publications* **30**, 85–94.

Veksler, I. V., Petibon, C. M., Jenner, G. A., Dorfman, A. M. & Dingwell, D. B. (1998). Partitioning of trace elements between immiscible silicate and carbonate liquids: an experimental study in the rotating centrifuge autoclave. *Journal of Petrology* **39**, 2095–2104.

Verwoerd, W. J. (1978). Liquid immiscibility and the carbonatite–ijolite relationship: preliminary data on the join $NaFe^{3+}Si_2O_6$–$CaCO_3$ and related compositions. *Carnegie Institution of Washington Yearbook* **77**, 767–774.

Wallace, M. E. & Green, D. H. (1988). An experimental determination of primary carbonatite magma composition. *Nature* **335**, 343–346.

Watkinson, D. H. & Wyllie, P. J. (1971). Experimental study of the join $NaAlSiO_4$–$CaCO_3$–H_2O and the genesis of alkalic rock–carbonatite complexes. *Journal of Petrology* **12**, 357–378.

Wendlandt, R. F. & Harrison, W. J. (1979). Rare earth partitioning between immiscible carbonate and silicate liquids and CO_2 vapour: results and implications for the formation of light rare-earth enriched rocks. *Contributions to Mineralogy and Petrology* **69**, 409–419.

Woolley, A. R. & Kempe, D.R. C. (1989). Carbonatites: nomenclature, average chemical compositions, and element distribution. In: Bell, K. (ed.) *Carbonatites: Genesis and Evolution*. London: Unwin Hyman, pp. 500–545.

Woolley, A. R. & Kjarsgaard, B. A. (2008). Paragenetic types of carbonatites as indicated by the diversity and relative abundances of associated silicate rocks: Evidence from a global database. *Canadian Mineralogist* **46**, 741–752.

Wyllie, P. J. (1989). Origin of carbonatites: Evidence from phase equilibrium studies. In: Bell, K. (ed.) *Carbonatites: Genesis and Evolution*. London: Unwin Hyman, pp. 500–545.

Wyllie, P. J. & Tuttle, O. F. (1960). The system CaO–CO_2–H_2O and the origin of carbonatites. *Journal of Petrology* **1**, 1–46.